Two-dimensional O(n) model in a staggered field

Dibyendu Das and Jesper Lykke Jacobsen

Laboratoire de Physique Théorique et Modèles Statistiques,
Université Paris-Sud, Bâtiment 100, F-91405 Orsay, France.

E-mails: das@ipno.in2p3.fr, jacobsen@ipno.in2p3.fr

Abstract.

Nienhuis' truncated O(n) model gives rise to a model of self-avoiding loops on the hexagonal lattice, each loop having a fugacity of n. We study such loops subjected to a particular kind of staggered field w, which for $n \to \infty$ has the geometrical effect of breaking the three-phase coexistence, linked to the three-colourability of the lattice faces. We show that at $T = 0$, for $w > 1$ the model flows to the ferromagnetic Potts model with $q = n^2$ states, with an associated fragmentation of the target space of the Coulomb gas. For $T > 0$, there is a competition between T and w which gives rise to multicritical versions of the dense and dilute loop universality classes. Via an exact mapping, and numerical results, we establish that the latter two critical branches coincide with those found earlier in the O(n) model on the triangular lattice. Using transfer matrix studies, we have found the renormalisation group flows in the full phase diagram in the (T, w) plane, with fixed n.

Superposing three copies of such hexagonal-lattice loop models with staggered fields produces a variety of one or three-species fully-packed loop models on the triangular lattice with certain geometrical constraints, possessing integer central charges $0 \le c \le 6$. In particular we show that Benjamini and Schramm's RGB loops have fractal dimension $D_{\rm f} = 3/2$.

1 Introduction

The O(n) model plays an important role in the realm of two-dimensional critical behaviour [1, 2, 3, 4]. In its lattice version, the partition function at temperature T reads

$$Z_{\mathrm{O}(n)} = \sum_{\{\vec{S}_i\}} \prod_{\langle ij \rangle} \exp\left(\frac{1}{T} \vec{S}_i \cdot \vec{S}_j \right), \tag{1.1}$$

where the $\vec{S}_i$ are n-component spins living on the vertices i of some regular two-dimensional lattice. The set of nearest-neighbour vertex pairs (lattice edges) is denoted by $\langle ij \rangle$.

From the high-temperature expansion, Z is linked to a model of loops, each loop having the fugacity n [1]. On the other hand, the O(n) model is related to standard ϕ^4 field theory, where the quartic term encodes the possibility of loop crossings [1, 2]. In two dimensions, this model possesses a second-order phase transition only for $|n| \le 2$. At the critical point, loop crossings are disfavoured, and in particular the limit $n \to 0$ gives access to the scaling properties of self-avoiding loops [1].

A related model can be obtained by truncating the high-temperature expansion as follows [3, 4]

$$Z_{\mathrm{loop}} = \sum_{\{\vec{S}_i\}} \prod_{\langle ij \rangle} \left(1 + \frac{1}{T} \vec{S}_i \cdot \vec{S}_j \right), \tag{1.2}$$

the model now being defined on a regular hexagonal lattice. The advantage of this truncation—and of the particular choice of the lattice—is that to all orders in the high-temperature expansion the loops become strictly self-avoiding. More precisely, one has

$$Z_{\mathrm{loop}} = T^{-N} \sum_{\mathcal{C}} n^{\mathcal{L}} T^{\mathcal{V}}, \tag{1.3}$$

where the summation is over configurations $\mathcal{C}$ of self-avoiding, mutually-avoiding loops on a hexagonal lattice of size N vertices. By construction, the number of loops passing through a given vertex is either zero or one. $\mathcal{L}$ denotes the number of loops in a given configuration, and $\mathcal{V}$ the number of vacancies, i.e., lattice vertices not visited by any loop.

The model defined by Z_{loop} is exactly solvable (in the sense of the Bethe Ansatz) along the curves [4, 5]

$$T^2 = 2 \pm \sqrt{2 - n}, \tag{1.4}$$

for $|n| \le 2$. Furthermore, it exhibits critical behaviour with algebraically decaying correlation functions. Its critical exponents along the curve $(1.4)^+$ are known exactly [4, 6, 7] and are believed to reproduce those of the generic O(n) model at its critical point T_{c}. We shall refer to this critical phase as that of *dilute loops*. The curve $(1.4)^-$ is to be understood as a line of renormalisation group fixed points that, for each $n \in (-2, 2)$, attract the whole low-temperature region $T \in (0, T_{\mathrm{c}})$. Also along this curve the critical exponents are known exactly [4, 8, 7]. We shall use the epithet *dense loops* to refer to the corresponding critical geometry.

However, the solution of Z_{loop} along $(1.4)^-$ does *not* describe the generic behaviour of the O(n) model in the low-temperature regime [9, 10]. The reason is that the model defined by Z_{loop} is unstable towards the inclusion of loop crossings. When included, these make the model flow to the generic symmetry-broken (Goldstone) phase of the ϕ^4 model,

which can in turn be described by supersymmetric methods [11, 9, 10]. Despite of this fact, Z_{loop} defines a very interesting model of self-avoiding loops and merits to be studied in detail on its own right.

Note that the sign of T in (1.4) is immaterial. This reflects the fact that, with suitable periodic boundary conditions, the number of vacancies is necessarily even. Thus, $T = 0$ constitutes another line of fixed points [12, 13], henceforth referred to as *compact loops*. This zero-temperature limit is once again exactly solvable [14, 15], and for $|n| \leq 2$ it is critical with exponents that are known exactly [15, 16]. From a geometrical point of view, this limit is particularly interesting since only the subset $\mathcal{C}_0 \subset \mathcal{C}$ of loop configurations in which the loops are *fully packed* contributes to Z_{loop}.

In this paper we shall study the hexagonal-lattice loop model (1.3) in the presence of a particular kind of staggered field[1] w. To define this field, we label the faces of the hexagonal lattice by integers $k = 1, 2, 3$ in such a way that any two adjacent faces carry different labels. Further define E_0 as the set of lattice edges whose two adjacent faces carry the labels 1 and 3. Given a loop configuration $\mathcal{C}$, let $\mathcal{F}$ be the number of edges in E_0 that are covered by a loop segment. The model to be studied is then defined by the partition function

$$Z = \sum_{\mathcal{C}} n^{\mathcal{L}} T^{\mathcal{V}} w^{\mathcal{F}}. \qquad (1.5)$$

Note that taking $w \neq 1$ does not break those of the lattice symmetries (translations and rotations) that respect the above sub-lattice structure. Thus, in the continuum limit we can hope to find further conformally invariant critical points for this model.

Our main objective is to identify the various critical behaviours of the model (1.5), and to study its phase diagram and renormalisation group flows with respect to the parameters n, T, and w. To this end we employ analytical arguments based on a Coulomb gas construction, exact mappings to related lattice models, and numerical transfer matrix results. In particular we show that, for $|n| \leq 2$, the model generically exhibits three more critical points than the dilute, dense, and compact loops invoked above. The first of these is encountered when $w \to \infty$ with $T = 0$, and we shall identify it as a $q = n^2$ state critical Potts model. The remaining two critical points are superpositions of a critical Ising model (free fermion) and dilute or dense loops, respectively.

The second part of the paper deals with fully-packed loop (FPL) models on the triangular lattice. The exact solutions of the FPL models on the hexagonal [15, 16] and the square [17] lattices imply that these models have different critical exponents. The reason for this non-universality can be traced back to a difference in the dimensionality of the target space of the corresponding Coulomb gases. Indeed, while the usual dense and dilute loop phases are described by the continuum limit of an interface model with a scalar height, the heights of the FPL model on the honeycomb (resp. square) lattice are vectors of dimension two (resp. three) [16, 17]. This motivates the study of FPL models on other lattices.

However, it is known numerically [18] that the standard FPL model on the triangular lattice[2] is in the same universality class as dense polymers [i.e., as the model (1.3) along

---

[1] In section 4 we shall give some justification for the nomenclature "staggered field" and discuss its relation to a similar construction in the Potts model.

[2] This is also true for a class of decorated lattices that interpolate between the square and the triangular

the curve $(1.4)^-$. It was pointed out in Ref. [20] that this type of flow from fully-packed loops to the low-temperature phase of the model (1.3) is indeed the generic scenario.

To avoid this flow, and to get new interesting critical behavior, one may subject the triangular-lattice loops to further constraints than just full packing. One such model, known as the RGB model, was introduced by Benjamini and Schramm [21] and studied numerically by Wilson [22]. In this model, the fully-packed loops are simply prohibited to take turns through an angle of $\pm\pi/3$ at any vertex; each loop carries a trivial fugacity of $n = 1$. However, the critical exponents of this model do not appear to have been determined [22].

Here we study several versions of such constrained FPL models on the triangular lattice, and we relate their critical exponents to those of the model (1.5). In particular, we establish that the fractal dimension of RGB loops is $D_\mathrm{f} = 3/2$.

The layout of the paper is as follows. In section 2 we introduce the model (1.5) and relate it to edge (Tate) colourings of the hexagonal lattice. We also show an exact mapping of our three-parameter model to a twelve-parameter loop model on the triangular lattice which has been studied earlier [23]. In section 3 we discuss the structure of the transfer matrix, which we use to obtain both analytical and numerical results. Section 4 gives some motivation for the introduction of the staggered field w, by comparing it to a similar construction for the Potts model. In section 5 we fix the notation by reviewing the Coulomb gas formalism for the FPL model at $w = 1$ [16]. We then show that for $w \to \infty$ the continuum limit of the FPL model coincides with that of a $q = n^2$ state Potts model. The same approach also reproduces known results for the finite temperature $\mathrm{O}(n)$ model [4]. In section 6 we discuss the results for the fixed points, critical surfaces, and renormalisation group flows in the full phase diagram in the (T, w) plane, at any fixed n. In section 7 we derive exact results for RGB loops on the triangular lattice [22], and for some generalisations thereof. We give our conclusions in section 8.

2 The model and some of its reformulations

Our loop model is defined on a hexagonal lattice with a set of special lattice edges E_0. If the faces of the hexagonal lattice are labeled by the integers $k = 1, 2, 3$ as shown in Fig. 1, then E_0 is the set of lattice edges between the faces labeled 1 and 3. On such a lattice, configurations $\mathcal{C}$ of self-avoiding, mutually-avoiding loops are laid down with weights given by Eq. (1.5).

In the present section we review various exact transformations relating this model to other discrete lattice models. These transformations become useful in later sections when we dress the Coulomb gas of the model (1.5) and examine its critical properties.

2.1 Three-colouring model

When $T = 0$, the subset $\mathcal{C}_0$ of configurations $\mathcal{C}$ which carry non-zero weight in Eq. (1.5) are those in which every vertex is visited by a loop. We shall refer to this as a fully-packed

lattices [19].

3

loops (FPL).

Such loops are related to the three-colouring model introduced by Baxter [14]. In this model, the edges of the hexagonal lattice are covered by colors A, B and C, subject to the constraint that no two edges of the same colour meet at a vertex. These colouring configurations can be brought into contact with FPL configurations as follows [14, 16].

Attribute an auxiliary orientation (clockwise or anti-clockwise) to each loop, and assign to each configuration $\mathcal{C}'_0$ of oriented loops a weight so that the Boltzmann factor of the corresponding un-oriented FPL configuration $\mathcal{C}_0$ is recovered by summing independently over the two possible orientations of each loop. Parametrising the loop weight n as[3]

$$n = \mathrm{e}^{6i\lambda} + \mathrm{e}^{-6i\lambda} = 2\cos(6\lambda), \tag{2.1}$$

this is accomplished by assigning a weight $\mathrm{e}^{6i\lambda}$ (resp. $\mathrm{e}^{-6i\lambda}$) to each clockwise (resp. anti-clockwise) oriented loop. To complete the mapping, a three-colouring configuration is identified bijectively with a oriented FPL configuration $\mathcal{C}'_0$ by letting the colour C (resp. B) represent a loop segment oriented from a vertex on the even sublattice to a vertex on the odd sublattice (resp. from odd to even). [We have here defined the even (resp. odd) sublattice as the vertices whose adjacent edges are dual to an up-pointing (resp. down-pointing) triangle.] The colour A means that there is no loop segment on the corresponding edge.

In this way, oriented loops become alternating sequences $BCBC\cdots$ or $CBCB\cdots$, depending on the orientation. Also note that violations of the FPL constraint (with weight T) correspond to defects in which three A colours meet at a vertex. Finally, to recover Eq. (1.5), a weight w is attributed to each E_0 edge carrying colour B or C. The correspondence between loops and colours is shown in Fig. 1.

The non-local loop weights can now be turned into local vertex weights, with respect to the three-colouring model, by assigning a weight $\mathrm{e}^{i\lambda}$ (resp. $\mathrm{e}^{-i\lambda}$) to each vertex where an oriented loop turns right (resp. left). The weights associated with the different vertex configurations are shown in Fig. 2. Assuming for the moment free boundary conditions, every closed loop turns ± 6 times more to the right than to the left, whence this re-assignment is compatible with Eq. (2.1).

The three-colouring model (with no defects, i.e., $T = 0$) can be mapped to a solid-on-solid model with a two-component microscopic height $z = (z_1, z_2)$ placed at the vertices of the triangular lattice dual to the hexagonal lattice. Details of this mapping can be found in Ref. [16], and are also shown in Fig. 2. When going from one vertex of the dual lattice to its neighbour, moving clockwise around an up-pointing (resp. down-pointing) triangle, z is incremented (resp. decremented) by the vector $\mathbf{A}$, $\mathbf{B}$, $\mathbf{C}$ depending on the colour of the direct-lattice edge being crossed. Adopting the normalisation of Ref. [16], one has

$$\mathbf{A} = \left(\frac{1}{\sqrt{3}}, 0\right), \qquad \mathbf{B} = \left(-\frac{1}{2\sqrt{3}}, \frac{1}{2}\right), \qquad \mathbf{C} = \left(-\frac{1}{2\sqrt{3}}, -\frac{1}{2}\right), \tag{2.2}$$

and since $\mathbf{A} + \mathbf{B} + \mathbf{C} = \mathbf{0}$ the height mapping is well-defined (up to a global shift) for each three-colouring configuration.

---

[3]We are mainly interested in $|n| \leq 2$, in which case λ is real [16]. For $n > 2$, λ is purely imaginary [14].
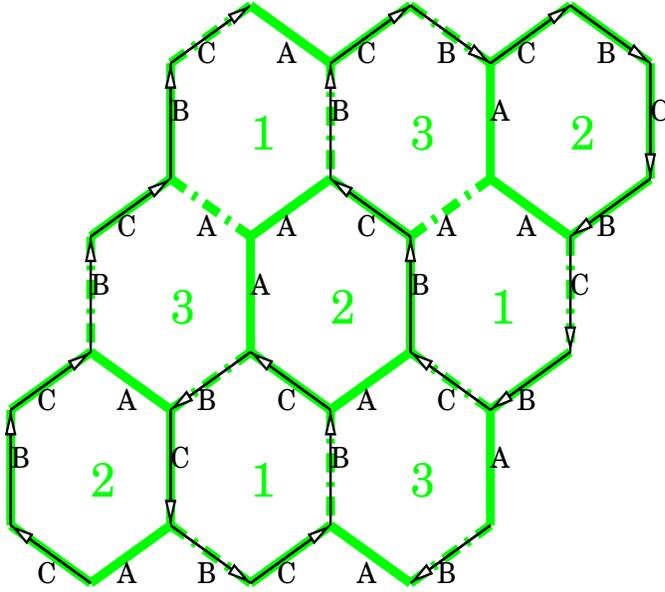
Figure 1: Loop configuration on the hexagonal lattice. The lattice faces are labeled by 1, 2 and 3 as indicated. Among the lattice edges (in grey), those separating 1 and 3-faces (broken linestyle) define the set E_0 (see text). Oriented loops (in black) live on lattice edges with colours B or C. Vertices where three A coloured edges meet break the fully-packing constraint.
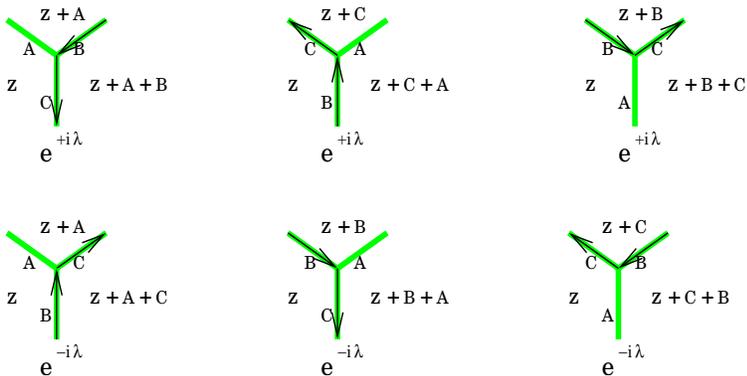

Figure 2: The microscopic height increments when crossing the coloured edges, here shown for an even vertex. We also give the local vertex weights, corresponding to all possible left and right turns of directed loop segments (shown as black arrows).
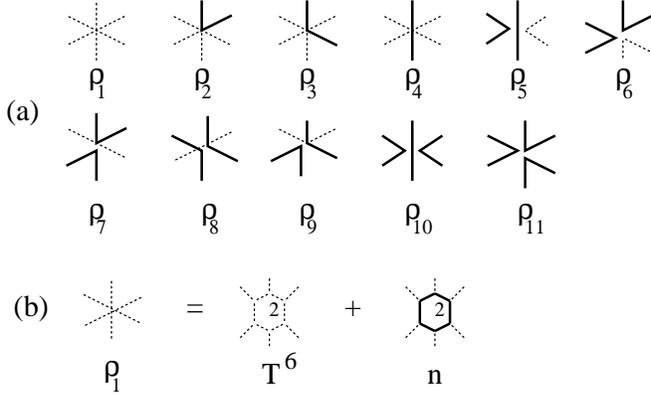
5

Figure 3: (a) Allowed vertices (up to rotations and reflections) of the triangular-lattice $O(n)$ model. The vertex weights ρ_i $(i = 1, 2, \ldots, 11)$ are defined in the figure. (b) As an example, it is shown how the summation over the two possible configurations around a 2-face, given that the six external legs are uncovered, leads to a vertex on the triangular lattice with weight $\rho_1 = T^6 + n$.

It is well-known that in the continuum limit this two-component height description reduces to a single-component height description when temperature defects are introduced ($T > 0$) [4]. Below, we shall show that this is also true—in a slightly more subtle way—when one has $T = 0$ and $w > 1$.

2.2 Decimation of 2-faces

The model (1.5) can be exactly mapped to a more involved loop model on the triangular lattice. To see this, consider shrinking the size of all the 2-faces in Fig. 1 to zero (alternatively this means shrinking all edges not in E_0 to zero). The result is a loop model on the triangular lattice in which loops are still non-crossing, but no longer self-avoiding, in the sense that a given vertex can be visited up to three times by the loops. Up to rotations and reflections, there are eleven local vertex configurations, as shown in Fig. 3.

The corresponding weights, denoted as $\rho_1, \rho_2, \ldots, \rho_{11}$, can be related to the three parameters T, w and n by summation over the internal structure (the shrunk 2-faces) of each triangular-lattice vertex. Note that all edges remaining after this shrinking are now of the E_0 type. Therefore, the weight w of an occupied edge can be redistributed by assigning $\sqrt{w}$ to each of the vertices at its extremities. The result is

$$
\begin{array}{lll}
\rho_1 = T^6 + n & \rho_2 = w(T^4 + 1) & \rho_3 = w(T^3 + T) \\
\rho_4 = 2wT^2 & \rho_5 = \rho_8 = w^2 & \rho_6 = \rho_7 = w^2 T^2 \\
\rho_9 = w^2 T & \rho_{10} = 0 & \rho_{11} = w^3
\end{array}
\tag{2.3}
$$

where, as usual, each closed loop carries a weight n.

The model defined by Fig. (3) is the triangular-lattice $O(n)$ model previously studied by Knops et al. [23], for general values of the weights ρ_k. The exact parametrisations of eight distinct branches of critical behaviour were conjectured as follows. First, both the

O(n) model itself and a certain Potts model on the hexagonal lattice (the latter having both edge and face interactions) were reformulated as spin-one 141-vertex models on the triangular lattice. The two 141-vertex models were then supposed to intersect exactly at the critical branches. The corresponding critical behaviour was then determined, in part by numerical simulations on the critical branches, and in part by analogy with an exact solution of the square-lattice O(n) model [24].

It is not a priori obvious whether this classification is complete. Actually this is not the case: for $T = 0$ and $w = 1$, the model (1.5) is known to have a compact loop phase [15, 16], which does not form part of the eight branches listed in Ref. [23].

The mapping (2.3) shows that the three-parameter phase space of the model (1.5) is a subset of the twelve-parameter phase space of the triangular-lattice O(n) model. In particular, in spite of our incomplete knowledge of the latter model, it seems likely that some of the critical branches identified in Ref. [23] are good candidates for further critical points of the model (1.5). We shall see below that these expectations are indeed fulfilled.

It is of course unlikely that a putative new critical point of the model (1.5) has vertex weights (2.3) that exactly coincide with one of the critical branches of the triangular-lattice O(n) model. However, it may still map to a point which *flows* to one of these branches under the renormalisation group (RG). Needless to say, it would be a tremendous task to elucidate the RG flows of the triangular-lattice O(n) model; for the model (1.5) this is however feasible (due to the vastly smaller number of parameters) and will be done below.

3   Transfer matrices

Before moving on to our analytical results for the model (1.5) we describe the construction of its transfer matrix. Understanding the conservation laws of the transfer matrix will be helpful in identifying the operators that are present in the continuum limit. Furthermore, diagonalising the transfer matrix numerically will serve as a check—and sometimes as a guideline—for the analytical results. We shall also use the numerical determination of the central charge and the critical exponents as an aid in dressing the complete phase diagram of the model, in section 6.

3.1   Basis states and algorithmic details

When dressing the transfer matrix for the model (1.5) a natural first question is how to deal with the non-local loop weights n. The solution to this problem is to work in a space of basis states containing non-local information about how the loop segments in a given time-slice were interconnected at former times [34]. The transfer matrix $\mathcal{T}$ time propagates the system by updating this connectedness information, and at the same time builds up the partition function.

The standard power method provides a convenient way of diagonalising $\mathcal{T}$. Namely, when letting $\mathcal{T}$ act repeatedly on a suitable reference state, the result will converge to the dominant eigenvector, and the rate of growth of the norm of the iterated state will yield the largest eigenvalue (which is non-degenerate by the Perron-Frobenius theorem).

The reference state is typically taken as one of the basis states. Care must be taken, however, since $\mathcal{T}$ is often block-diagonal due to the existence of conservation laws (see below). In this case, one must ensure that the reference state belongs to the same block as the dominant eigenvector.

The power method also allows for extracting sub-dominant eigenvalues, by iterating several states which are kept mutually orthogonal after each iteration.

One can think of the entries of $\mathcal{T}$ as being indexed by a pair of integers (row and column number). Relating these integers to the connectedness information which constitutes the basis states is technically involved [34], and is once again linked to the issue of conservation laws. Fortunately, this complication can be eliminated completely by characterising each state by a large integer (which is usually easy) and inserting the states generated at each iteration into a hash table.

Finally, the efficiency of the transfer matrix algorithm is optimised by using a sparse matrix factorisation scheme, in which $\mathcal{T}$ is written as a product of matrices which each add a single vertex to the lattice.

3.2   Conservation laws

We now examine the conservation laws associated with the transfer matrices for strips of finite width L of the lattice model (1.5).

On the hexagonal lattice there are two natural transfer (or time-like) directions, $\mathcal{T}_\parallel$ and $\mathcal{T}_\perp$, which are respectively parallel ($\mathcal{T}_\parallel$) and perpendicular ($\mathcal{T}_\perp$) to one third of the lattice edges. In Fig. 1, $\mathcal{T}_\parallel$ is vertical and $\mathcal{T}_\perp$ is horizontal. With periodic transverse boundary conditions, the minimal number of dangling edges L for these two choices are respectively $3k$ and $2k$ (with k being an integer) in the ground state sector. (In other words, as a function of L we can expect the various eigenvalues to exhibit "mod 3" and "mod 2" fluctuations respectively. The ground state sector is such that periodic transverse boundary conditions respect the sublattice structure of the hexagonal lattice.)

In the FPL model (with $T = 0$), for the direction $\mathcal{T}_\parallel$ the number of edges that are occupied by loop segments (i.e., the number of B colours plus the number of C colours) is conserved [14]. For entropic reasons, we can expect the largest eigenvalue to reside in the sector with the largest number of configurations, which is then the one with loop density $2/3$. If there are $2l$ occupied loop segments in a strip of size $L = 3k$, then the number of states in the sector is

$$\binom{3k}{2l} c_l, \tag{3.1}$$

where $c_l = (2l)!/[l!(l + 1)!]$ are the Catalan numbers. For the direction $\mathcal{T}_\perp$, the conserved quantity is $Q = $ [the number of loop segments on even edges] minus [the number of loop segments on odd edges]. This can be easily checked by considering the action of the transfer matrix on all possible states of an even edge and the adjacent odd edge. For $Q = 2q$, the number of states in the sector labeled by Q is

$$\sum_{l=0}^{k-2q} \binom{k}{l + 2q}\binom{k}{l} c_{l+q}. \tag{3.2}$$

Namely, out of the available $2k$ edges, one has to choose l occupied odd edges and $l+2q$ occupied even edges. These can then finally be interconnected in c_{l+q} ways. The largest eigenvalue is expected to reside in the $Q=0$ sector.

Taking $T>0$, these conservation laws are modified. For instance, in the $\mathcal{T}_\parallel$ direction it is now the difference of the up and down oriented vertical loop segments (i.e., the number of B colours minus the number of C colours) which is conserved.

3.3   Series expansions

We further note that in the large-n limit, for $w<1$ and $w>1$, the first few terms of the series expansion for the free energy per face can be easily written down:

$$
\begin{aligned}
-f_{w<1} &= \frac{1}{3}\ln\, n + \frac{2w^3}{3n^2} + O(\frac{1}{n^4}) \\
-f_{w>1} &= \frac{1}{3}\ln\, n + \ln\, w + \frac{1}{3n^2}(1+\frac{1}{w^3}+\cdots) + O(\frac{1}{n^4}).
\end{aligned}
\tag{3.3}
$$

Comparing these series expansions with our numerically obtained free energies (see below) provides a useful check of our algorithms.

3.4   Eigenvalues and critical exponents

The central charge c and the scaling dimensions x_i of various correlation functions can be extracted from the transfer matrix spectra in a standard way. Let the eigenvalues be labeled as $\Lambda_0 > \Lambda_1 \geq \Lambda_2 \geq \ldots$ (the first few dominant eigenvalues turn out to be real and positive). One can obtain c and the x_i from [35, 36]

$$
f_0(L) = f(\infty) - \frac{\pi c}{6L^2} + o\left(L^{-2}\right)
\tag{3.4}
$$

and [37]

$$
f_i(L) - f_0(L) = \frac{2\pi x_i}{L^2} + o\left(L^{-2}\right).
\tag{3.5}
$$

Here the free energy per unit area reads $f_0 = -A\ln(\Lambda_0)/(LM)$, where $M \gg 1$ is the number of rows of the strip; we similarly relate f_i to Λ_i. The geometrical factor A reads $A = 2/\sqrt{3}$ for the $\mathcal{T}_\parallel$ direction and $A = \sqrt{3}/2$ for the $\mathcal{T}_\perp$ direction; it ensures that the free energy is properly normalised per unit area.

3.5   The case $T=0$, $w\to\infty$

Consider now the transfer direction $\mathcal{T}_\parallel$ in the case of $T=0$ and $w\to\infty$. In Fig. 4 we show a small portion of the lattice between two time slices; the transfer direction is here understood to be vertical. The E_0 edges are marked on the figure, and in any allowed configuration these must be covered by loop segments.

We now focus on the two non-E_0 vertical edges in the bottom of Fig. 4. Using the fully-packing constraint—and the fact that all E_0 edges must be occupied—it is easy to
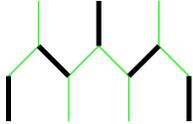
Figure 4: A small portion of the hexagonal lattice between two time slices; the transfer direction is vertical. The E_0 edges are shown in black.
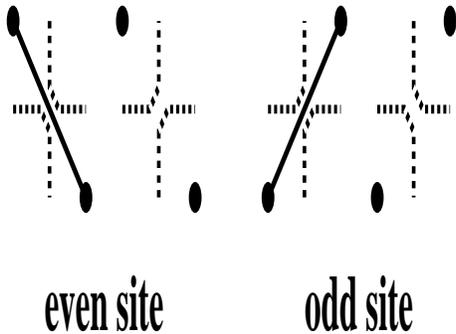

even site   odd site

Figure 5: The Potts model as a loop model on the square lattice. The circles represent the Potts spins, the solid lines are bonds in the clusters, and the broken lines are loop segments.

see that if these two edges are both unoccupied one arrives at a contradiction. The same is true if they are both occupied. Therefore, exactly one of them must be occupied. This implies that the only allowed sector of the transfer matrix is the one in which *exactly* 2/3 of the vertical edges are covered.

The ground state sector has $3k$ vertical edges in each time slice. The number of covered vertical edges is therefore $2k$, i.e., even.

4   The staggered field

In the introduction, it was claimed that the parameter w in Eq. (1.5) can be considered as a staggered field. To make this more clear, we wish to compare it with a similar construction in the Potts model.

One of the nicest reformulations of the square-lattice q-state Potts model is as a loop model on the square lattice [38]. It is well-known that the Potts model can be transformed into a random cluster model, where the summation over Potts spins is turned into a summation over bond-percolation clusters [25]; each cluster connects vertices whose spins are in the same state. This can be further transformed into a loop model in which the loops bounce off the boundaries (both exterior and interior) of the clusters, and of the dual clusters. This construction is illustrated in Fig. 5.

The partition function is then proportional to

$$Z_{\text{Potts}} = \sum_{\text{loops}} q^{\mathcal{L}/2} u^{\mathcal{B}}, \tag{4.1}$$

where $\mathcal{L}$ is the number of closed loops and $\mathcal{B}$ is the number of edges covered by a bond of the clusters. The parameter $u = (e^K - 1)/\sqrt{q}$, where K is the reduced spin-spin coupling in the Potts model. According to Fig. 5, the correspondence between the weight u and the local behaviour of the loops at the clusters depends on the sublattice. In this sense, u is a staggered field. Also note that the selfdual point is at $u = 1$, and only in this case is the model exactly solvable [38].

Now consider the limit $q \to \infty$, with $u = 1$. There are just two dominant configurations, each with the same weight, in which loops of length four encircle the even (resp. the odd) faces of the lattice. In terms of the spins these are the completely ordered (ferromagnetic) and the completely disordered (paramagnetic) states. Moving u away from 1 will favour one of these configurations. Thus, the selfdual manifold $u = 1$ can be considered as a two-phase coexistence curve, even for finite q. For $q > 4$ this phase coexistence is first order: taking u through 1 drives the system through a first order thermal phase transition with non-vanishing latent heat [26]. For $q \leq 4$ the coexistence becomes second order, and $u = 1$ is indeed the (ferromagnetic) critical point of the Potts model. Even in this latter case, taking $u \neq 1$ will favour one of the phases and induce an RG flow that will take the system to either of the two reference configurations, i.e., to non-criticality.

Our motivation for introducing the model (1.5) is taken from the above scenario. The parameter w is a staggered field in the above sense. Consider first the case of $T = 0$. When $n \to \infty$ with $w = 1$, there is a coexistence between *three* dominant configurations, in which loops of length six encircle the faces labeled $k = 1, 2, 3$ respectively.

In Fig. 6 we illustrate a domain wall between faces $k = 1$ and $k = 3$, for $n \gg 1$. The states on either side of the domain wall can be thought of as completely ordered phases of a three-state Potts model, with spins in the state k being placed at the centres of the small loops. Let us write its hamiltonian as follows:

$$\mathcal{H}_{3-\text{Potts}} = -K \sum_{\langle ij \rangle} \delta_{\sigma_i, \sigma_j} - H \sum_i (1 - \delta_{\sigma_i, 2}). \tag{4.2}$$

The Potts spins $\sigma_i = 1, 2, 3$ thus live on a triangular lattice, which is however slightly shifted across the domain wall. To ensure full packing, a single long loop is necessary to separate the phases. The space taken up by the domain wall is delimited by the two black curves. In the ordered phases, per Potts spin there is one loop of weight n and three satisfied couplings K. Therefore[4]

$$K \sim \frac{1}{3} \log n. \tag{4.3}$$

Taking $w \neq 1$ similarly induces a magnetic field H in the three-state Potts model (4.2), with

$$H \sim 3 \log w. \tag{4.4}$$

---

[4]Note that when $q \to \infty$, the loop model based on the q-state Potts model can be similarly related to an Ising model. The simple argument above then leads to the relation $K_{\text{Ising}} = \frac{1}{8} \log q$; this was found in Ref. [27] by a more complicated argument, which involved counting the length of the domain wall.
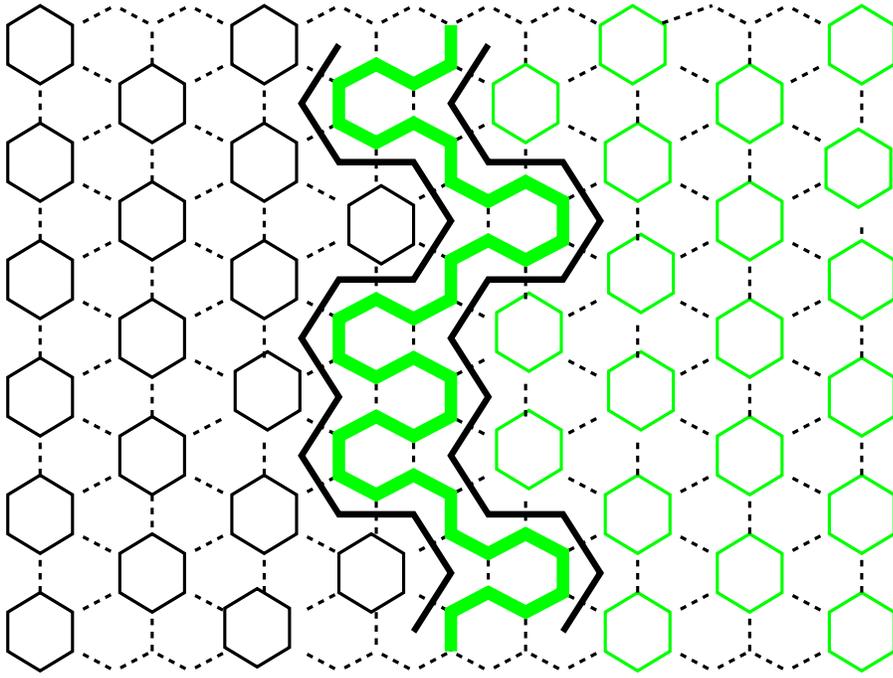
Figure 6: The space between the two black curves is filled up by a domain wall (thick grey loop segment) that separates two domains of phase 1 (black loops, on the left) and phase 3 (grey loops, on the right). Potts spins lie at the centres of the hexagons, i.e., on two triangular lattices, which have a slight mismatch.
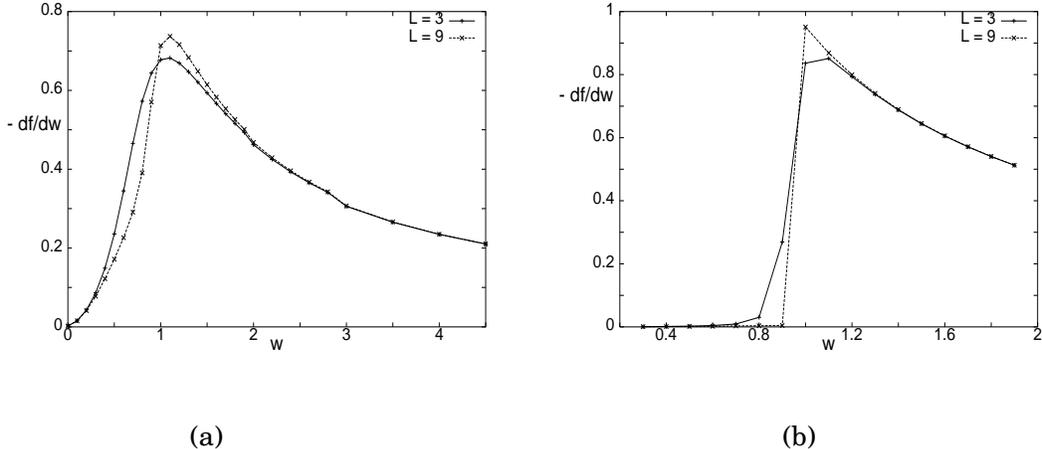
Figure 7: (a) The derivative $-df/dw$ at $w = 1$ is continuous for $n = \sqrt{3}$. (b) The derivative is discontinuous at $w = 1$ for $n = 20$.

For n finite, the curve $w = 1$ can still be considered as the three-phase coexistence curve. Since the correlation length for $w = 1$ is known to be finite for $n > 2$ and infinite for $n \leq 2$ [14, 15, 16], it seems natural to expect that taking w through 1 will induce a first-order transition for $n > 2$ and a second-order transition for $n \leq 2$. This expectation is confirmed in Fig. 7 by numerically evaluating the derivative of the free energy density f with respect to w, using the transfer matrix $\mathcal{T}_{\parallel}$ for strips of various widths L.

The staggered field w can be expected to have a richer behaviour than in the Potts case. Namely, for $w > 1$ the three-phase coexistence is broken down to two-phase coexistence (rather than just to a trivial one-phase "coexistence", which happens for $w < 1$). This means that it is still possible to find some critical behaviour for $w > 1$; in section 5 we shall describe exactly how this comes about.

Consider finally the case of finite temperature $T > 0$. The parameter T acts so as to avoid full packing, while w tries to enforce it. There is thus some hope that the competition between w and T may lead to interesting multicritical behaviour. This gives rise to a rather rich phase diagram, which will be investigated in section 6.

5 Coulomb gas formalism

The critical phases of loop models can be described in terms of effective field theories. Exploiting the various symmetries at both the microscopic and coarse-grained levels, one can construct such theories, and obtain the central charge and critical exponents exactly via the Coulomb gas correspondence [29, 16, 17].

In section 5.1 we begin by reviewing the case of compact loops ($T = 0$ and $w = 1$), following Refs. [16, 17]. Apart from fixing the notation, this will also serve as a basis for section 5.2, in which we obtain the central charge and the critical exponents for $w > 1$. In section 5.3, we show how the same formalism gives back the known results [4] for the case of $T > 0$ and $w = 1$.

13

5.1 FPL model at $w = 1$

The effective field theory for the long-wavelength behaviour of the model is written in terms of a coarse-grained height field, obtained from the microscopic height z already defined above.

A typical configuration of the critical oriented FPL model, considered in terms of the colouring model, has domains of *ideal states*, which are colouring states having the least possible variance of z. In other word, ideal states are macroscopically flat. In an ideal state, all loops have length six and the same orientation: as each loop can be oriented in two ways, there are six such states. To each of them we assign a coarse-grained height $\mathbf{h} = (h_1, h_2) = \langle z \rangle$, which is the average microscopic height over a $\sqrt{3} \times \sqrt{3}$ unit cell of the colouring.

The dominant contributions to the free energy are bounded fluctuations around these flat states, as they maximise the local entropy density. In the continuum limit, the height is assumed to be a smooth function of the $2-$dimensional coordinates (x^1, x^2). The part of the partition function accounting for the large scale fluctuations, namely $Z_> = \int \mathcal{D}\mathbf{h} \exp(-S[\mathbf{h}])$, has an Euclidean action S with three terms:

$$S = S_{\mathrm{E}} + S_{\mathrm{B}} + S_{\mathrm{L}}. \tag{5.1}$$

In Fig. 8, we show the positions of the ideal states in the coarse-grained height space. The hexagonal lattice with sides $\frac{1}{3}$ having the ideal states at the vertices is referred to as the *ideal state graph* $\mathcal{I}$. The nodes of $\mathcal{I}$ that correspond to the same ideal state, form a triangular lattice with sides 1, and is referred to as the *repeat lattice* $\mathcal{R}$.

Below we list some important height differences associated with symmetry transformations between a pair of ideal states, the order being that of increasing norm. The vectors $\mathbf{m}_1^c = \frac{1}{3}(\mathbf{A} - \mathbf{C})$ and $\mathbf{m}_2^c = \frac{1}{3}(\mathbf{B} - \mathbf{A})$ (the superscript c indicates 'colour') have norm $\frac{1}{3}$; they are associated with elementary colour exchanges $A \leftrightarrow C$ and $A \leftrightarrow B$, respectively; these vectors span a hexagonal lattice. The vectors $\mathbf{m}_1^r = \mathbf{C}$ and $\mathbf{m}_2^r = \mathbf{A}$ (the superscript r indicates 'rotation') have norm $\frac{1}{\sqrt{3}}$; they are associated with transformation of one ideal state to another via 120° spatial rotation; they span a triangular lattice. Finally, the vectors $\mathbf{m}_1^R = (\mathbf{C} - \mathbf{B})$ and $\mathbf{m}_2^R = (\mathbf{A} - \mathbf{C})$ (the superscript R stands for 'repeat') with norm 1 form the basis of the triangular repeat lattice $\mathcal{R}$; they are associated with transforming the ideal states back on to themselves.

Each of the terms in Eq. (5.1) can be interpreted from geometrical and symmetry considerations.

The first term S_{E} is due to the *elastic fluctuations* of the interface, and has terms in gradient-square of the height field. Imposing translational and rotational symmetry at the coarse-grained level, the general form of this term must be $\int \mathrm{d}^2 x \, \{K_{11}(\boldsymbol{\partial} h_1)^2 + K_{22}(\boldsymbol{\partial} h_2)^2 + K_{12}(\boldsymbol{\partial} h_1) \cdot (\boldsymbol{\partial} h_2)\}$, where $\boldsymbol{\partial} = (\partial_1, \partial_2)$ is the usual gradient. Due to colour exchange symmetries at the microscopic level, there are some constraints on these coupling constants. First, the symmetry $B \leftrightarrow C$ changing the loop orientation corresponds to $z_2 \leftrightarrow -z_2$, $z_1 \leftrightarrow z_1$ in Eq. (2.2) and keeps the weights in Fig. 2 invariant if we let $\lambda \leftrightarrow -\lambda$. This implies that $K_{12} = 0$. Second, the cyclic exchange of colours $A \to B \to C$ corresponds to $z_1 \to -\frac{1}{2}z_1 - \frac{\sqrt{3}}{2}z_2$, $z_2 \to \frac{\sqrt{3}}{2}z_1 - \frac{1}{2}z_2$ and leaves the weights unchanged.
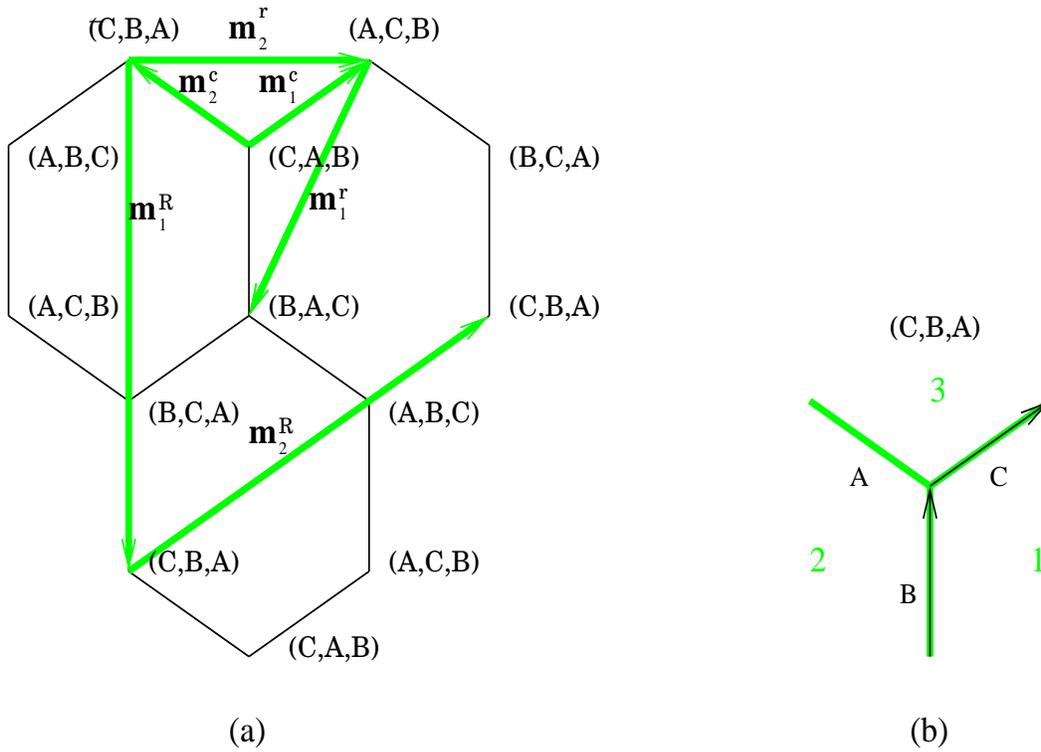
Figure 8: (a) The ideal state graph $\mathcal{I}$ shows the relative positions of the different ideal states in the coarse-grained height space. (b) The labeling of an ideal state—here (C, B, A)—is the ordered list of edge colours around an even vertex, with face labels as shown (starting from the rightmost edge, and turning clockwise around the vertex). The vectors $\mathbf{m}_1^c$, $\mathbf{m}_2^c$, $\mathbf{m}_1^r$, $\mathbf{m}_2^r$, $\mathbf{m}_1^R$ and $\mathbf{m}_2^R$ are defined in the text.

15

This implies $K_{11} = K_{22}$; we shall denote this common value by $g\pi$ henceforth.[5] Thus,

$$S_E = \int d^2\mathbf{x} \exp\left(g\pi\{(\boldsymbol{\partial}h_1)^2 + (\boldsymbol{\partial}h_2)^2\}\right). \tag{5.2}$$

The mapping of the loop model to an oriented loop model with local complex weights as defined in section 2 does not work for loops which experience the boundary. For example if the model is defined on a cylinder, an oriented loop winding around the cylinder will pick up a total weight of *one* since it makes an equal number of left and right turns. Summing over the two orientations there is a weight of 2 for the loop, whereas, by definition of the model, every loop should have an weight n. To correct for this, one introduces a *background term* S_B in the action:

$$S_B = \frac{i}{2} \int d^2\mathbf{x}(\mathbf{e}_0 \cdot \mathbf{h})\tilde{\mathcal{R}}. \tag{5.3}$$

In the above, $\tilde{\mathcal{R}}$ is the scalar curvature of the space on which the model is defined, and $\mathbf{e}_0$ is the *background electric charge*, yet to be determined.

On the cylinder, the scalar curvature is zero, except at the two boundaries at infinity along the cylinder axis, so that $S_B = \exp(2\pi i\mathbf{e}_0 \cdot (\mathbf{h}(x^1, +\infty) - \mathbf{h}(x^1, -\infty)))$; we have here taken x^2 to denote the time-like coordinate. The unique solution that attributes the correct phase $e^{\pm 6i\lambda}$ to every winding oriented loop reads

$$\mathbf{e}_0 = (0, e_0) = \left(0, \frac{6\lambda}{\pi}\right) = \left(0, \frac{1}{\pi}\cos^{-1}(n/2)\right). \tag{5.4}$$

The terms in the action described so far constitute a Coulomb gas [30] with two bosonic fields h_1 and h_2, where h_2 is coupled to a background charge $-2e_0$. A crucial role is played by the last *Liouville term* in the action, which reads

$$S_L = \int d^2\mathbf{x}\, W[\mathbf{h}(\mathbf{x})], \tag{5.5}$$

where $\exp(-W[\mathbf{h}(\mathbf{x})])$ is the scaling limit of the complex weights at any vertex, namely $\exp(\pm i\lambda)$ as discussed before. We list below the microscopic weights W with respect to colorings around the vertex using the notation of Fig. 8(*b*) and Eq. (5.4):

$$W(C, A, B) = W(B, C, A) = W(A, B, C) = +i\frac{\pi}{6}e_0$$

$$W(C, B, A) = W(B, A, C) = W(A, C, B) = -i\frac{\pi}{6}e_0 \tag{5.6}$$

The microscopic operator $W(\mathbf{x})$ is *uniform* in each ideal state, and is a function of the height $\mathbf{h} \in \mathcal{I}$. Since it is a periodic function of $\mathbf{h}(\mathbf{x})$ it can be written as a Fourier series,

$$W[\mathbf{h}(\mathbf{x})] = \sum_{\mathbf{e}\in\mathcal{R}_W^*} \tilde{W}_{\mathbf{e}} \exp(i2\pi\mathbf{e} \cdot \mathbf{h}(\mathbf{x})). \tag{5.7}$$

In the continuum limit, this becomes a sum of vertex operators, and $\mathbf{e}$ are the corresponding electric charges which belong to a lattice $\mathcal{R}_W^* \subset \mathcal{R}^*$. Here, $\mathcal{R}^*$ is the reciprocal

---

[5] We have here sticked to the notation of Ref. [16]. To compare our formulae with Ref. [17], one needs to replace g by $K/2\pi$ and $\mathbf{e}$ by $\mathbf{e}/2\pi$.

of the repeat lattice $\mathcal{R}$, and $\mathcal{R}_w^*$ is the lattice reciprocal to the lattice of *periods* of $W(\mathbf{h})$. We now determine which vertex operators in Eq. (5.7) are the most relevant; these are the only ones to be kept in the action.

In a Coulomb gas, operators are associated with electric and magnetic charges. Electric charges $\mathbf{e}$ are linked to the periodicity of the height field, and appear in the vertex operators (spins waves) $\exp(i2\pi\mathbf{e}\cdot\mathbf{h})$, as discussed in Eq. 5.7. Magnetic charges $\mathbf{m}$ are the topological charges of vortex defects in the height. Within the Coulomb gas formalism, the scaling dimension of a general operator with electric and magnetic charges $\mathbf{e}$ and $\mathbf{m}$ is computed as [31]

$$x(\mathbf{e}, \mathbf{m}) = \frac{1}{2g}\mathbf{e}\cdot(\mathbf{e} - 2\mathbf{e}_0) + \frac{g}{2}\mathbf{m}\cdot\mathbf{m}. \tag{5.8}$$

The lattice $\mathcal{R}$ is spanned by the vectors $\mathbf{m}_1^R = (0, -1)$ and $\mathbf{m}_2^R = (\frac{\sqrt{3}}{2}, \frac{1}{2})$. The corresponding reciprocal lattice $\mathcal{R}^*$ is hexagonal, and we denote its six shortest vectors by $\mathbf{e}^R$. For future reference, we list here these vectors as well as the scaling dimensions (found from Eq. (5.8) with $\mathbf{m} = \mathbf{0}$) of the corresponding vertex operators:

$$
\begin{array}{lll}
\mathbf{e}_1^R = \frac{2}{\sqrt{3}}\left(\frac{1}{2}, \frac{-\sqrt{3}}{2}\right), & \mathbf{e}_4^R = \frac{2}{\sqrt{3}}\left(\frac{-1}{2}, \frac{-\sqrt{3}}{2}\right) & x(\mathbf{e}_1^R) = x(\mathbf{e}_4^R) = \frac{\frac{4}{3}+2e_0}{2g} \\
\mathbf{e}_2^R = \frac{2}{\sqrt{3}}(1, 0), & \mathbf{e}_5^R = \frac{2}{\sqrt{3}}(-1, 0) & x(\mathbf{e}_2^R) = x(\mathbf{e}_5^R) = \frac{\frac{4}{3}}{2g} \\
\mathbf{e}_3^R = \frac{2}{\sqrt{3}}\left(\frac{1}{2}, \frac{\sqrt{3}}{2}\right), & \mathbf{e}_6^R = \frac{2}{\sqrt{3}}\left(\frac{-1}{2}, \frac{\sqrt{3}}{2}\right) & x(\mathbf{e}_3^R) = x(\mathbf{e}_6^R) = \frac{\frac{4}{3}-2e_0}{2g}
\end{array} \tag{5.9}
$$

To find the electric vectors appearing in the expansion (5.7), we note that the loop-weight operator $w(\mathbf{h})$ has a higher periodicity than that of $\mathbf{m}^R$. Namely, the microscopic weights (5.6) of the ideal states are invariant with with respect to 120° rotations, which are linked to the periodicity of $\mathbf{m}^r$. Thus, the lattice $\mathcal{R}_W$ determining the periodicity of the weights is spanned by the vectors $\mathbf{m}_1^r$ and $\mathbf{m}_2^r$ of Fig. 8. The corresponding reciprocal lattice $\mathcal{R}_W^*$ is hexagonal, and its shortest vectors $\mathbf{e}^r$ and the scaling dimensions of the corresponding vertex operators are as follows:

$$
\begin{array}{ll}
\mathbf{e}_1^r = 2(0, -1) & x(\mathbf{e}_1^r) = \frac{4+4e_0}{2g} \\
\mathbf{e}_2^r = 2\left(\frac{\sqrt{3}}{2}, \frac{-1}{2}\right), \quad \mathbf{e}_3^r = 2\left(\frac{-\sqrt{3}}{2}, \frac{-1}{2}\right) & x(\mathbf{e}_2^r) = x(\mathbf{e}_3^R) = \frac{4+2e_0}{2g} \\
\mathbf{e}_5^r = 2\left(\frac{-\sqrt{3}}{2}, \frac{1}{2}\right), \quad \mathbf{e}_6^r = 2\left(\frac{\sqrt{3}}{2}, \frac{1}{2}\right) & x(\mathbf{e}_5^r) = x(\mathbf{e}_6^r) = \frac{4-2e_0}{2g} \\
\mathbf{e}_4^r = 2(0, 1) & x(\mathbf{e}_4^r) = \frac{4-4e_0}{2g}
\end{array} \tag{5.10}
$$

We see that the most relevant vector is $\mathbf{e}_4^r$, and it is sufficient to keep only the corresponding vertex operator in Eq. (5.7).

It has been argued in Refs. [16, 17] that since the loop weight does not flow under the renormalisation group, the corresponding continuum operator $W[\mathbf{h}(\mathbf{x})]$ must be exactly marginal. In other words, the screening charge of the Coulomb gas is the electric vector corresponding to the most relevant vertex operator in the expansion (5.7). We therefore set $x(\mathbf{e}_4^r) = 2$, and as a consequence the coupling constant g gets fixed as a function of e_0 (and hence n):

$$g = 1 - e_0. \tag{5.11}$$

By virtue of Eq. (5.11), all the critical exponents and the central charge for the system now gets determined exactly.[6]

---

[6]The compactification radius of the boson h_2 is the repeat lattice unit vector length ($= 1$) and does

The central charge of the critical FPL model is obtained by noting that there are two bosonic fields h_1 and h_2, where h_1 is free and h_2 is coupled to the background charge $-2e_0$. This is given as [31, 16]

$$c = 2 + 12x(\mathbf{e}_0, \mathbf{0}) = 2 - \frac{6e_0^2}{1 - e_0}. \tag{5.12}$$

The thermal dimension x_T, describing the algebraic decay of the energy-energy correlator, is linked to a magnetic charge. Namely, thermal fluctuations breaking the FPL constraint create pairs of vertices not covered by loops, as shown in Fig. 9(a). In the height model these are vortices with magnetic charge $\mathbf{m} = 3\mathbf{A} = (\sqrt{3}, 0)$ and zero electric charge. Eqs. (5.8) and (5.11) immediately give,

$$x_T = \frac{3}{2}(1 - e_0). \tag{5.13}$$

Note that the electric charges $\mathbf{e}^R$ and $\mathbf{e}^r$ that could have been candidates for the thermal operator are ruled out: the former because it does not respect the periodicity of the weights, and the latter because it is irrelevant (and in particular less relevant than (5.13)).

Similarly, the one-string and the two-string defects, shown in Fig. 9(b) and (c), correspond to vortices with magnetic charges $\mathbf{m}_1 = 2\mathbf{A} + \mathbf{B} = (\frac{\sqrt{3}}{2}, \frac{1}{2}) = \mathbf{m}_2^R$ and $\mathbf{m}_2 = \mathbf{A} + 2\mathbf{B} = (0, 1) = -\mathbf{m}_1^R$ respectively.[7] At each vortex core there is an additional electric charge $\mathbf{e}_0$, whose role is to cancel the spurious phase factors arising when the strings wind around the core [29]. The corresponding scaling dimensions x_1 and x_2 thus read

$$x_1 = x_2 = \frac{(1 - e_0)}{2} - \frac{e_0^2}{2(1 - e_0)}. \tag{5.14}$$

The generalisation to k-string defects is given in Ref. [16]. Note that the correlation function of a two-string defect propagating from $\mathbf{0}$ to $\mathbf{r}$ is proportional to the probability of having a loop passing through the points $\mathbf{0}$ and $\mathbf{r}$, and that the two-string dimension is related to the fractal dimension D_f of the loop via the relation [32, 33],

$$D_f = 2 - x_2. \tag{5.15}$$

5.2 FPL model for $w \neq 1$

Having reviewed the known results for the FPL model with $w = 1$, we now show how the results get modified for $w \neq 1$, primarily because of the change of symmetries. We expect that the fixed point at $w = 1$ is repulsive, and since the symmetry-breaking effect of taking $w \neq 1$ does not compete with any other parameter (note that we still have $T = 0$) is seems unlikely that the RG flow will halt at any finite value of w. We

---

not appear explicitly in the dimension formula (Eq. (5.8)) due to our choice of the units of the vectors $\mathbf{A}$, $\mathbf{B}$ and $\mathbf{C}$. But even if such a parameter were retained, the product of it with g would get fixed as in Eq. (5.11).

[7]Note that in order for the height mapping to be globally defined, the total magnetic charge of the vortices must vanish. In particular, this implies that the vortex and the anti-vortex that participate in a two-point correlation function of the thermal or the one-string type must reside at *opposite* sublattices. This is not so for the two-string type correlation function; see Fig. 9(b).
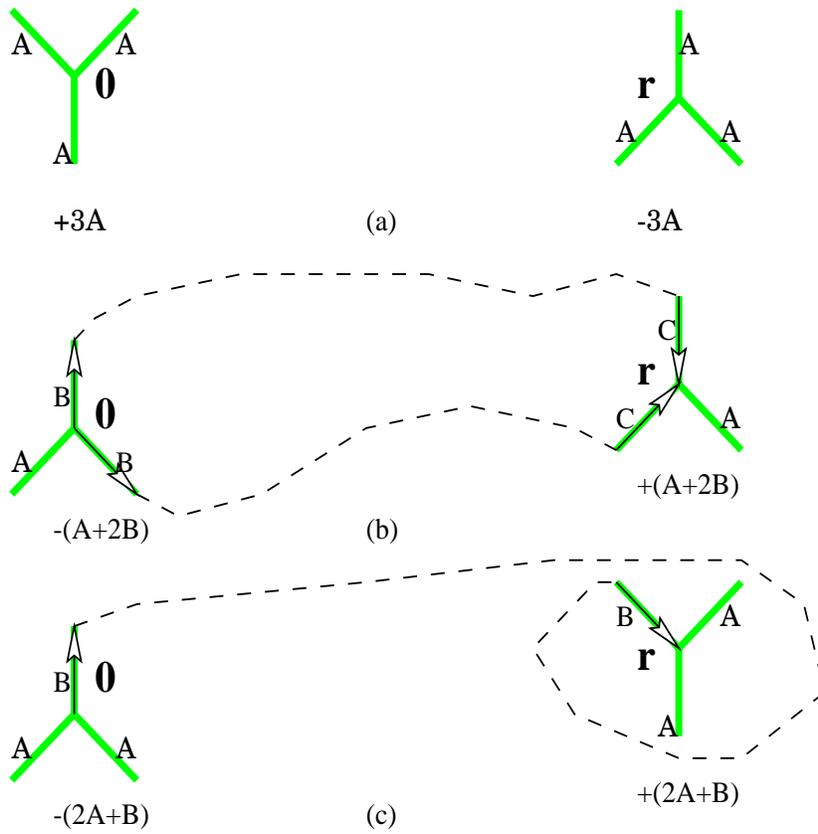
Figure 9: Pairs of thermal defects (a), two-string defects (b), and one-string defects (c) at the positions **0** and **r**. The dashed lines denote the paths of open $BCBC\cdots$ strings. In (c) the defect string winds around the vortex core (see text).

therefore anticipate a flow towards fixed points at $w = 0$ and $w = \infty$ respectively; these expectations are confirmed by our numerical results and the subsequent analysis.

The fixed point at $w = 0$ is trivial, as the only allowed FPL configuration is the one in which small loops turn around the 1-faces, avoiding all the E_0 edges; cf. Fig. 1. Clearly, this state cannot be critical.

The situation for $w \to \infty$ is more interesting. Even though the loops have to cover all the E_0 edges, and stay fully packed, there are many available configurations. We shall see below that the ideal state graph $\mathcal{I}$ gets fragmented, new electric vectors emerge, and that for $|n| \leq 2$ the $w = \infty$ fixed point is in the same universality class as the critical $q = n^2$ state Potts model.

We begin by examining the ideal state graph in Fig. 8. In the limit $w \to \infty$, the two ideal states (A, B, C) and (A, C, B) are suppressed, as they correspond to colours A lying on top of the E_0 edges. We have however checked that for a large lattice with suitable periodic boundary conditions there exists a sequence of microscopic updates (permutation of two colours around a closed loop) that link the four remaining ideal states:

$$(C, B, A) \to (C, A, B) \to (B, A, C) \to (B, C, A) \to (C, B, A) \to \cdots, \tag{5.16}$$

where all the intermediate configurations in the sequence have the loops covering all the E_0 edges. Indeed, transforming (C, A, B) into (B, A, C) requires interchanging colours B and C, and this is easily achieved by successively flipping the direction of all the BC-type loops. Transforming (B, A, C) into (B, C, A) is more interesting. Flipping first an AC-type loop of length 6 will create a BC-type loop of length 18. This latter loop can be made bigger by flipping further AC-type loops that touch its perimeter. Continuing in this way, the BC-type loop will eventually go to the boundary of the system (and thus annihilate, due to the periodic boundary conditions), and the region at its interior will transform into the ideal state (B, C, A), as required.

This means on one hand that the two-dimensional ideal state graph in Fig. 8(a) becomes fragmented, and on the other hand that the four remaining possible ideal states forming a valid quasi one-dimensional ideal state graph. The repeat lattice is now one-dimensional, and is spanned by the vector $\mathbf{m}_1^R$, as shown in Fig. 10(a).

Let us consider what this change implies for the three terms in the action (5.1). Of the various symmetries used to reduce the number of parameters in the elastic tensor, only the cyclic exchange of colours $A \to B \to C$ fails. This means that K_{11} and K_{22} can now be different. In fact, the structure of $\mathcal{I}$, as shown in Fig. 10(a), suggests that the fluctuations of the first height component h_1 is suppressed, and $K_{11} \to \infty$. Denoting $K_{22} = \pi g$ the elastic term therefore takes the form

$$S_{\mathrm{E}} = \int \mathrm{d}^2\mathbf{x} \, \exp\left(g\pi(\boldsymbol{\partial} h_2)^2\right). \tag{5.17}$$

The argument giving the boundary term S_{B} is unchanged. So the the bosonic field h_2 is again coupled to the background charge $-2e_0$ given by Eq. (5.4).

The Liouville term S_{L} is still given by Eqs. (5.5) and (5.7), but the microscopic vertex weights (5.6) are replaced by:

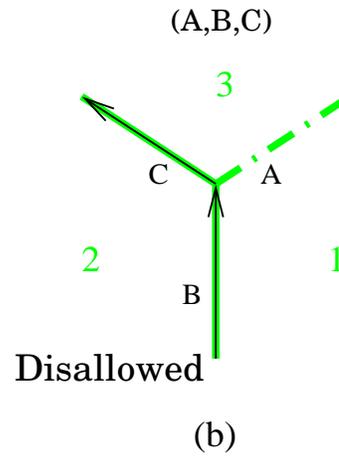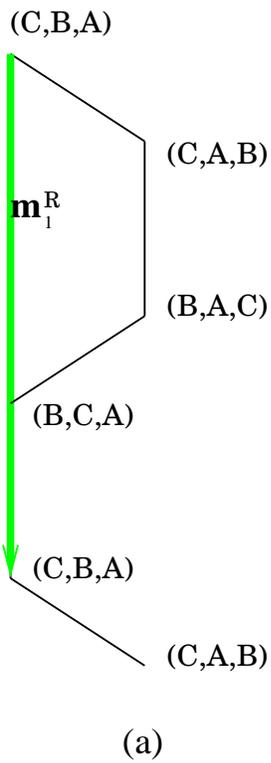$$W(C, A, B) \;=\; W(B, C, A) = +i\frac{\pi}{6}e_0$$

20

Figure 10: (a) The quasi one-dimensional ideal state graph of the $T = 0$, $w \to \infty$ model. (b) The state (A, B, C) is disallowed as no loop passes over the edge shared by the faces labeled 1 and 3.

$$W(C, B, A) = W(B, A, C) = -i\frac{\pi}{6}e_0$$

$$W(A, B, C) = +i\frac{\pi}{6}e_0 - \ln[w]$$

$$W(A, C, B) = -i\frac{\pi}{6}e_0 - \ln[w] \tag{5.18}$$

The crucial thing to note is that the invariance under 120° rotations of the ideal states has been lost.

All of the symmetry-related lattices (the ideal state graph, the repeat lattice, and so on) should now be considered as one-dimensional, as should the electric and magnetic charges. To see this, consider writing the analogue of Eq. (5.8) with couplings $K_{11} \neq K_{22}$. In the limit $K_{11} \to \infty$, the first component of $\mathbf{e} = (e_1, e_2)$ becomes immaterial, and any non-zero first component in $\mathbf{m} = (m_1, m_2)$ would lead to an infinite scaling dimension, whence the corresponding operator is infinitely irrelevant. The change from a two- to a one-dimensional lattice will actually modify the computation of electric charges, even if in some cases they are still reciprocal to the same height periods as before. To avoid confusion, we shall therefore denote the one-dimensional electric charges by the letter $\mathbf{G}$ in the following.

The repeat lattice is now spanned by $\mathbf{m}_1^R = (0, -1)$. The shortest vectors in $\mathcal{R}^*$ and the dimensions of the corresponding vertex operators read, by Eq. (5.8):

$$\begin{array}{ll} \mathbf{G}_1^R = (0, -1) & x(\mathbf{G}_1^R) = \frac{1+2e_0}{2g} \\ \mathbf{G}_2^R = (0, 1) & x(\mathbf{G}_2^R) = \frac{1-2e_0}{2g} \end{array} \tag{5.19}$$

The next-shortest vectors in $\mathcal{R}^*$ are $\mathbf{G}_1^r = 2\mathbf{G}_1^R = 2(0, -1)$ and $\mathbf{G}_2^r = 2\mathbf{G}_2^R = 2(0, 1)$. These are also the shortest vectors in $\mathcal{R}_W^*$. To see this, consider the one-dimensional projection of the ideal state graph shown in Fig. 10. Due to the equality of weights in the first two lines of Eq. (5.18), the weight operator is periodic with half the period of the repeat lattice.

Interestingly, the electric charges $\mathbf{G}_1^r$ and $\mathbf{G}_2^r$ coincide with $\mathbf{e}_1^r$ and $\mathbf{e}_4^r$ in Eq. (5.10); the other $\mathbf{e}^r$'s are now absent. The marginality of the weight operator therefore still leads to $x(\mathbf{e}_4^r) = 2$, and the same fixation of the coupling, $g = (1 - e_0)$, as in Eq. (5.11).

Since there is now only a single bosonic field coupled to the background charge $-2e_0$, we get the central charge as

$$c = 1 - \frac{6e_0^2}{1 - e_0}. \tag{5.20}$$

We next turn to the thermal exponent. A height defect of magnetic charge $3\mathbf{A}$ is no longer allowed, as this would mean leaving an E_0 edge uncovered. This suggests that the energy operator is linked to an electric charge instead. We claim further that the appropriate vertex operator is expected to have the same periodicity as the vertex weights (5.18), since the latter encode the energy of the various microscopic configurations (note that these "energies" are purely imaginary in the oriented loop model). The candidate electric charges are given by Eq. (5.19), and they also happen to be the shortest vectors of $\mathcal{R}^*$ (and hence correspond to the most relevant vertex operators). From this argument one should think that $x_T = x(\mathbf{G}_2^R)$; however, our numerical results unambiguously show

that the correct identification is

$$x_T = x(\mathbf{G}_1^R) = \frac{1 + 2e_0}{2(1 - e_0)}. \tag{5.21}$$

It is seen from Eqs. (5.20)–(5.21) that the critical FPL model at $w \to \infty$ is in the same universality class as the $q = n^2$ Potts model. The Coulomb gas of the Potts model is known to exhibit a so-called charge asymmetry [29, 23], which explains the seemingly paradoxical identification of x_T with $x(\mathbf{G}_1^R)$, rather than with $x(\mathbf{G}_2^R)$ whose vertex operator is more relevant.

The two-string defect dimension x_2 associated with the magnetic charge $\mathbf{m}_1^R = (0, -1)$ and the fractal dimension D_f are still given by Eqs. (5.14) and (5.15).

String defects with any *odd* number of strings, however, do not exist at the fixed point under consideration. This is not surprising, since the magnetic charges of such defects lead to infinite scaling dimensions, as explained above. Note also that in the standard formulation of the critical Potts model as a loop model on the square lattice, strings can be identified as the boundaries of Fortuin-Kasteleyn clusters [38], cf. section 4. Thus, in terms of the Potts spins an odd number of string is meaningless.

Yet another argument for the absence of string defects with an odd number of strings can be obtained by considering the transfer matrix in the direction $\mathcal{T}_\|$, in the limit $w \to \infty$. In section 3.5 we have showed that the conserved number of occupied vertical edges in a time-slice must be *even*. Clearly, this rules out the possibility of having states with a single string, and any number of pairwise connected loop segments.

We conclude this section by presenting some numerical evidence for the correctness of the above predictions. In Fig. 11 we show the effective central charge c_eff for the $T = 0$ model, as a function of w, for various system sizes L. The data for different values of n all agree to show a global maximum at $w = 1$. By Zamolodchikov's c-theorem [28] this means a repulsive fixed point, just as expected. The repulsive nature is further confirmed by the fact that the peak gets sharper as the system size increases.

When $w < 1$, the RG flow goes all the way down to $w = 0$, which is the location of the trivial fixed point discussed above. Here, $c_\mathrm{eff} = 0$, indicating non-critical behaviour.

When $w > 1$, c_eff rapidly attains a plateau, which extends all the way to $w = \infty$. This indicates an RG flow towards a fixed point at $w = \infty$. The nature of this fixed point is attractive, as witnessed by the fact that the plateau gets broader and flatter with increasing system size.

Finally note that the values of the central charge at the fixed points $w = 1$ and $w = \infty$ are in excellent agreement with the predictions of Eqs. (5.12) and (5.20) respectively.

We have also checked the values of the thermal exponent x_T at the fixed point $w = \infty$. We here coded our transfer matrix so that only configurations in which loops covering all the E_0 edges were allowed. This led to a reduction in the number of configurations, and hence exploration of larger system sizes. We list in Table 1, the exponents (obtained from Eq. (3.5)) as a function of system size for different n, and compare them with the x_T given by Eq. (5.21). The agreement is very good, in particular when allowing for some extrapolation of the finite-size data.
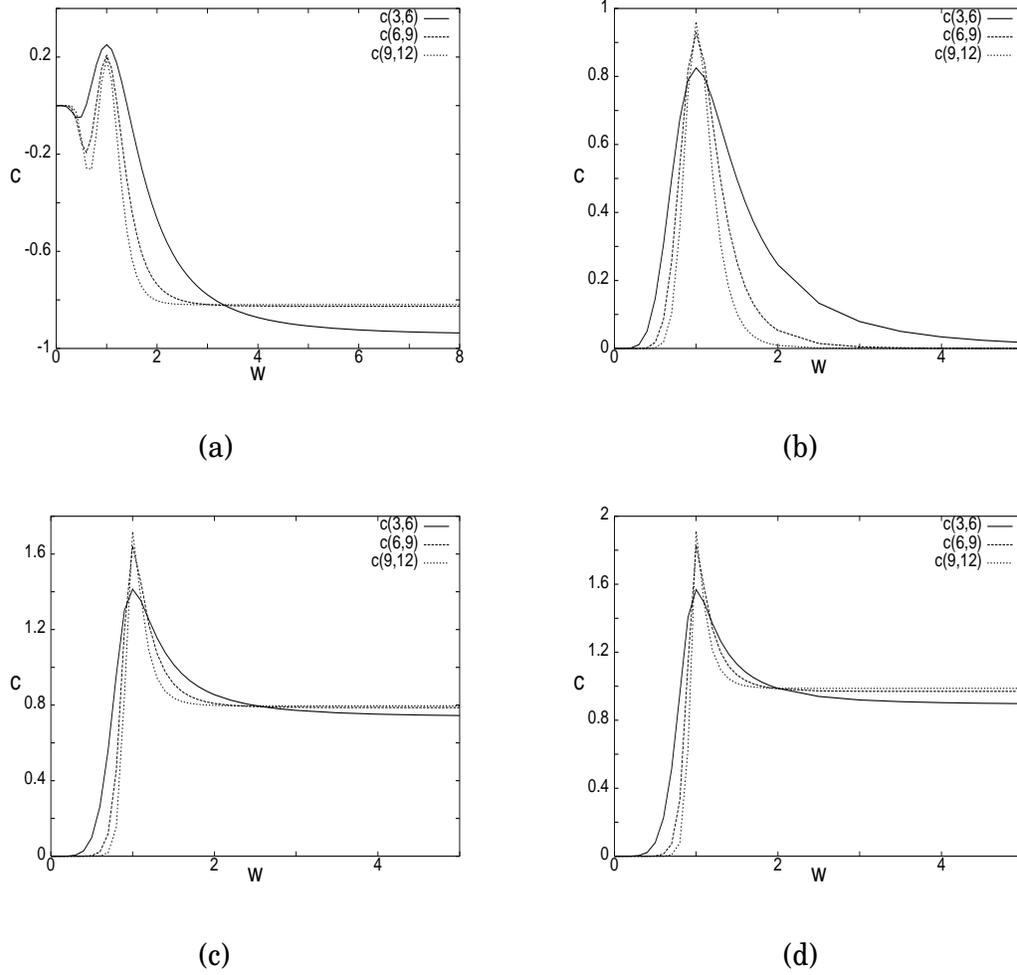
(a)

(b)

(c)

(d)

Figure 11: The central charge c as a function of w for different n: (a) $n = 1/2$, (b) $n = 1$, (c) $n = \sqrt{3}$, and (d) $n = 2$. All the curves are obtained using the two-parameter fits of Eq. (3.4).

n	$L = 6$	$L = 9$	$L = 12$	$L = 15$	$L = 18$	Exact
2.0	0.5592	0.5482	0.5439	0.5417	0.5403	0.5
$\sqrt{3}$	0.7166	0.7265	0.7360	0.7436	0.7496	0.8
$\sqrt{2}$	0.9981	0.9996	0.9999	1.0000	1.0000	1
1.0	1.5286	1.3716	1.3141	1.2898	1.2772	1.25
0.5	0.9466	1.3112	1.3996	1.4588	1.4959	1.5842882

Table 1: Thermal exponent x_T in the limit $w \to \infty$.

5.3   Finite temperature, $w = 1$

Let us now show how the same formalism developed for the FPL models above, can be used to rederive the known results for the $w = 1$ model at finite temperature [4]. The crucial difference with the FPL model is that there is now a finite density of the vertex configurations shown in Fig. 9(a), where three A colours meet. Since these are defects of magnetic charge $\Delta \mathbf{h} = 3\mathbf{A} = (\sqrt{3}, 0)$, this makes the two-dimensional height model break down. More precisely, this suggests that h_1 fluctuations are suppressed, and that the model must be described in terms of the h_2 component only. In particular, the ideal state graph again becomes quasi one-dimensional.

Let us first discuss the generic effective field theory, i.e., at an arbitrary but small value of T. The elastic term and the background term in the action are given now for the bosonic field h_2 by Eqs. (5.17) and (5.3). The local loop weight operator gets modified due to the new weights of uncovered vertices:

$$
\begin{aligned}
w(C, A, B) &= w(B, C, A) = w(A, B, C) = +i\frac{\pi}{6}e_0 \\
w(C, B, A) &= w(B, A, C) = w(A, C, B) = -i\frac{\pi}{6}e_0 \\
w(A, A, A) &= -\ln[T]
\end{aligned}
\tag{5.22}
$$

This implies that the coarse-grained loop weight operator (5.7) is invariant under all $120°$ rotations. The most relevant electric vector is again $\mathbf{G}_2^r = \mathbf{e}_4^r = 2(0, 1)$. The marginality assumption leads to $x(\mathbf{e}_4^r) = 2$, implying $g = 1 - e_0$. This leads to the central charge being given again by Eq. (5.20).

The thermal exponent is linked to an electric charge in the Coulomb gas, since going to a one-dimensional height has projected to zero the magnetic charge formerly linked with a temperature-like defect of three A colours. The most relevant vertex operators have electric charge $\mathbf{G}_1^R$ and $\mathbf{G}_2^R$. However, these are ruled out since they do not have the full symmetry of the weights (5.22) with respect to $120°$ rotations. The next available choices are $\mathbf{G}_1^R$ and $\mathbf{G}_2^R$, of which the latter is already in use as the screening operator. By Eq. (5.10) we therefore have

$$
x_T = x(\mathbf{G}_1^R) = \frac{2(1 + e_0)}{1 - e_0}.
\tag{5.23}
$$

With $0 \le e_0 < 1$, corresponding to $2 \ge n > -2$, this is indeed the correct result for dense polymers [4]. Note also that $x_T > 2$, so that temperature is indeed irrelevant at this fixed point.

Note that the above argument did not in any way use the exactly known location of the critical point $(1.4)^-$. The temperature enters in various non-universal quantities, such as the coefficients $\tilde{W}_\mathbf{e}$ in Eq. (5.7). It therefore may happen at a *particular* value of T that $\tilde{W}_{\mathbf{G}_2^r} = 0$. We conjecture that this happens at the critical temperature T_c, given by Eq. $(1.4)^+$. The screening charge is then $\mathbf{G}_1^r$, and setting $x(\mathbf{G}_1^r) = 2$ we obtain $g = 1 + e_0$. Hence

$$
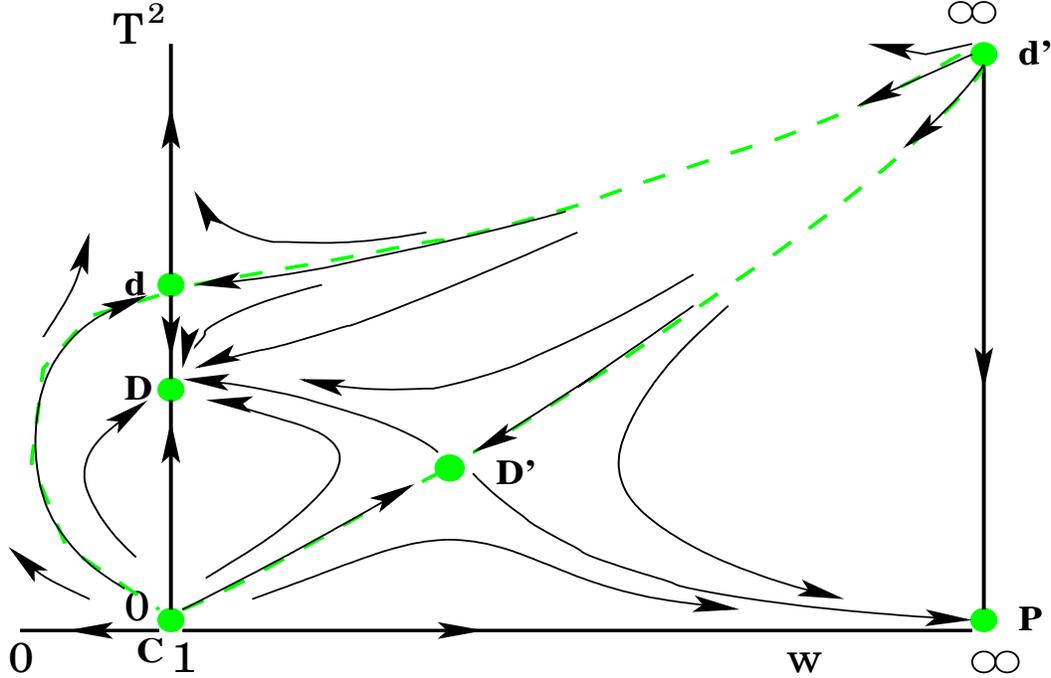c = 1 - \frac{6e_0^2}{1 + e_0},
\tag{5.24}
$$

Figure 12: The schematic phase diagram for the $O(n)$ model on the hexagonal lattice in the (w, T^2) plane at fixed $n \in (0, 2)$. Grey filled circles indicate critical fixed points; for the point at (∞, ∞) see the text. The renormalisation group flows are sketched by black arrows. The interpretation of the various critical points is as follows (see text for details): C compact loops; D dense loops; d dilute loops; P Potts model; D' tricritical dense loops; d' tricritical dilute loops.

and the thermal operator

$$x_T = x(\mathbf{G}_2^R) = \frac{2(1 - e_0)}{1 + e_0} \tag{5.25}$$

is now relevant, as it should. Note that Eqs. (5.24)–(5.25) can also be obtained from Eqs. (5.20) and (5.23) by analytic continuation, i.e., by taking $-1 < e_0 \leq 0$, which once again corresponds to $-2 < n \leq 2$ [4].

6 Phase diagram

6.1 Fixed points and renormalisation group flows

In Fig. 12 we show the schematic phase diagram for the model (1.5) in the (w, T^2) plane at a fixed value of n. This diagram is valid for $0 \leq n < 2$. The case $n = 2$ is slightly special and will be discussed separately in section 6.4.

The critical fixed points C (compact loops), D (dense loops) and d (dilute loops), were previously known and have been discussed in the introduction. The direction of the RG flows for $w = 1$ follow from the relevance (resp. irrelevance) of x_T at C and d (resp. at D).

Note also the agreement with the c-theorem [28], according to which the effective central charge decreases along RG flows.

In section 5.2 we have demonstrated that for $T = 0$ there is a flow from C to another fixed point P (Potts model) situated at $w = \infty$.

It should be noted that the points D and P are both generic in the sense that their Coulomb gas is one-dimensional with no tunable parameters. (In particular, their central charges coincide.) This would seem to indicate that these points should be attractive in all directions. In the case of D this is supported by the irrelevance of the temperature perturbation, i.e., $x_T > 2$ in Eq. (5.23). In the case of P, we have seen in section 5.2 that $1/w$ is irrelevant. It is also true that T is irrelevant. This can be seen, on one hand, microscopically by noticing that the $w \to \infty$ limit enforces full packing for any finite T. On the other hand, one has formally $x(\mathbf{0}, \mathbf{3A}) = \infty$ in Eq. (5.8), cf. the remark after Eq. (5.18). Thus finite T is indeed infinitely irrelevant at P.[8]

Accepting the attractive nature of D and P in all directions in the (w, T^2) plane as a working hypothesis, there must be a curve emanating from C that separates their respective basins of attraction. For the qualitative reasons given towards the end of section 4, it seems reasonable to suppose there will be an RG flow along this curve, going from C towards a new multicritical point D' situated at finite T and w.

The simplest way of obtaining a phase diagram that is consistent with the properties listed above is to suppose the existence of yet another fixed point d' at infinite T and w, which is repulsive in all directions in the (w, T^2) plane. This yields then the conjectured phase diagram shown in Fig. 12. The limit $w, T \to \infty$ should be taken with $\lambda \equiv T^2/w$ fixed, since uncovering an E_0 edge will necessarily lead to the formation of two empty vertices. Taking $\lambda \to 0$ we recover an FPL model, i.e., the point P. On the other hand, $\lambda \to \infty$ yields a completely empty configuration. The hypothesis is thus that there exists a critical fixed point d' situated at some finite value $\lambda = \lambda_c$.

6.2 Universality classes and numerical results

To verify the hypotheses made above—and to establish the universality classes of the proposed fixed points D' and d'—we proceed to make some numerical checks.

To get some guidance, we show in Fig. 13 a plot of the effective central charge c_{eff} (i.e., the value of c obtained by fitting the numerically obtained free energies to Eq. (3.4) for two different system sizes L) as a function of T, at fixed $n = \sqrt{3}$ and $w = 1.60$. At $T = 0$, with increasing system size L we have $c_{\text{eff}} \to 4/5$, in agreement with the prediction for the point P, cf. Eq. (5.20). At $T = T^-(w) \simeq 0.39$, one observes a maximum in c_{eff}. This is the signature of the line of RG flows that separates the basins of attraction of D and P in Fig. 12. This is followed by a plateau in c_{eff} signaling the basin of attraction of D. The broadening of this plateau with increasing L is consistent with the attractive nature of

---

[8]This statement is seemingly contradicted by the fact that $x_T < 2$ at P [see Eq. (5.21)]. However, we remind that the notation x_T refers to the scaling dimension of the energy operator, which is related to the next-largest translationally invariant eigenvalue of the transfer matrix. This does not necessarily coincide with the operator that couples to the temperature variable T. Thus, the exponent x_T of Eq. (5.21) must correspond to one of the nine independent way of leaving the manifold (2.3) which embeds the model (1.5) within the more general triangular-lattice $O(n)$ model.
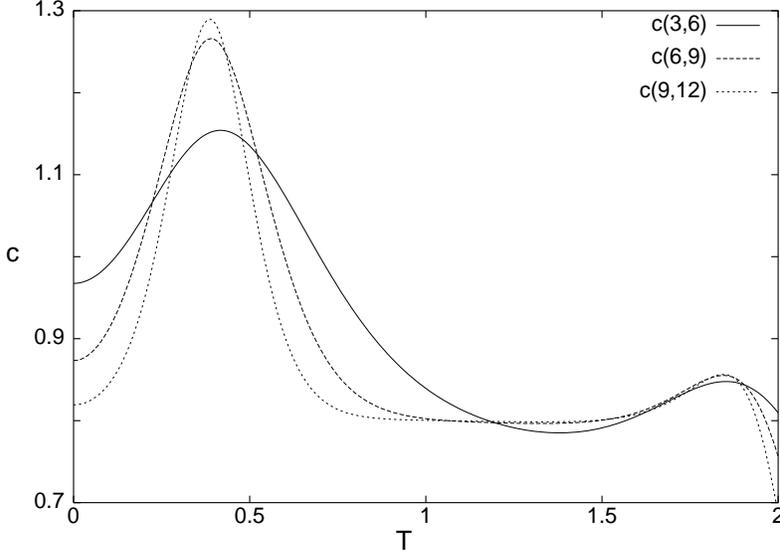
Figure 13: Plot of c_{eff} versus T at $n = \sqrt{3}$ and $w = 1.60$, for various system sizes L. The two maxima are at $T^-(w) \simeq 0.39$ and $T^+(w) \simeq 1.84$.

D. Moreover, the plateau value $c_{\text{eff}} \simeq 4/5$ is in agreement with the prediction for D. At $T = T^+(w) \simeq 1.84$, the plateau terminates in a second maximum. This is the signature of the line of RG flows that separates the basins of attraction of D and the trivial fixed point at $(w, T^2) = (0, \infty)$. For $T > T^+$, c_{eff} levels off to zero, signaling non-critical behaviour. Note that the sharpening of the two maxima at $T^{\pm}(w)$ with increasing L is consistent with the corresponding RG flows' being repulsive in the temperature direction.

The curves $c_{\text{eff}}(T)$ have a similar functional form (two maxima separated by a plateau) for other values of w. This enables us to determine the curves $T^{\pm}(w)$ for any fixed value of n. In Table 2 we show the results for $T^-(w)$ at $n = \sqrt{3}$. Extrapolations to the limits $w \to 1$ and $w \to \infty$ confirms that this RG separatrix connects the points C and d' in Fig. 12. Actually, we expect $T^-(w)$ to diverge as $w^{1/2}$ when $w \to \infty$, since d' is located

w	$c(3,6)$	$c(6,9)$	$c(9,12)$	$T^-(w)$
1.60	1.1541	1.2660	1.2895	0.39 ± 0.01
2.00	1.1847	1.2762	1.2921	0.56 ± 0.01
3.30	1.2206	1.2838	1.2943	0.99 ± 0.01
3.42	1.2204	1.2839	1.2943	1.028 ± 0.001
3.50	1.2200	1.2838	1.2942	1.05 ± 0.01
4.00	1.2158	1.2832	1.2941	1.19 ± 0.01
6.00	1.1919	1.2786	1.2930	1.66 ± 0.01

Table 2: Low-temperature maxima of $c_{\text{eff}}(T)$, as a function of system size L, for various values of w and fixed $n = \sqrt{3}$. We also show the estimates of $T^-(w)$, extrapolated to the $L \to \infty$ limit.

at finite $\lambda = T^2/w$. Examining now the variation of $c_{\text{eff}}(T^-(w))$, we observe a maximum at

$$w_{\text{c}} = 3.42 \pm 0.01 \quad \text{and} \quad T^-(w_{\text{c}}) = 1.028 \pm 0.001 \qquad (n = \sqrt{3}). \tag{6.1}$$

This is our estimate of the location of the point D', here for $n = \sqrt{3}$. Note that the maximum gets broader with increasing L, in agreement with the attractive nature of D' along the separatrix; see Fig. 12. Extrapolating the corresponding central charge to $L \to \infty$ we obtain

$$c_{\text{D}'}(n = \sqrt{3}) = 1.304 \pm 0.005. \tag{6.2}$$

We have repeated this analysis for $n = \sqrt{2}$, finding similar qualitative results. The point D' is here located at

$$w_{\text{c}} = 3.60 \pm 0.01 \quad \text{and} \quad T^-(w_{\text{c}}) = 1.030 \pm 0.001 \qquad (n = \sqrt{2}), \tag{6.3}$$

and the central charge reads

$$c_{\text{D}'}(n = \sqrt{2}) = 1.004 \pm 0.005. \tag{6.4}$$

The mapping from the model (1.5) to the triangular-lattice O(n) model [23] exhibited in section 2.2 makes it plausible that the points D' and d' should coincide with critical behaviour found in the latter model. We therefore conjecture that the universality class of D' is that of a superposition of dense loops and a critical Ising model, referred to as branch 5 in Ref. [23]. This means

$$c = \frac{3}{2} - \frac{6e_0^2}{1 - e_0}. \tag{6.5}$$

$$x_T = 1, \tag{6.6}$$

since the thermal exponent of the Ising model is always more relevant than that of dense loops.

This conjecture for c is in excellent agreement with Eqs. (6.2) and (6.4). The numerical estimates for $x_T(L)$ read, for $n = \sqrt{3}$,

$$x_T(6) = 0.8622, \quad x_T(9) = 0.8782, \quad x_T(12) = 0.8880. \tag{6.7}$$

For $n = \sqrt{2}$ we find

$$x_T(6) = 0.9920, \quad x_T(9) = 0.9973, \quad x_T(12) = 0.9986. \tag{6.8}$$

The agreement with Eq. (6.6) is reasonable for $n = \sqrt{3}$ (the finite-size corrections are strong), and excellent for $n = \sqrt{2}$.

Following the second maximum in Fig. 13 allows us similarly to trace out the curve $T^+(w)$. The result is shown in Table 3. This separatrix is seen to connect the points d and, quite plausibly, d'. Once again we expect $T^+(w)$ to behave as $w^{1/2}$ when $w \to \infty$, and this is confirmed by the data in Table 3. Furthermore, the variation of c_{eff} with L is now consistent with d being attractive along the separatrix, exactly as shown in Fig. 12.

We have also followed the maxima in Fig. 13 into the region $0 \le w < 1$. We find that for a certain value $w = w_0$ the two maxima coalesce, and for $w < w_0$ the model is

w	$c(3,6)$	$c(6,9)$	$c(9,12)$	$T^+(w)$
1.04	0.859630	0.856344	0.856625	1.6079 ± 0.0001
1.08	0.859414	0.856323	0.856622	1.6277 ± 0.0001
1.12	0.859065	0.856291	0.856616	1.6471 ± 0.0001
1.20	0.858011	0.856190	0.856599	1.6847 ± 0.0001
1.60	0.847764	0.855149	0.856392	1.845 ± 0.001
2.00	0.833671	0.853567	0.856042	1.967 ± 0.001
4.00	$--$	0.843420	0.853420	2.456 ± 0.005
6.00	$--$	0.836064	0.850333	2.80 ± 0.02

Table 3: High-temperature maxima of $c_{\mathrm{eff}}(T)$, as a function of system size L, for various values of w and fixed $n = \sqrt{3}$. We also show the estimates of $T^+(w)$, extrapolated to the $L \to \infty$ limit.

n	$c(3,6)$	$c(6,9)$	$c(9,12)$	$c(12,15)$	λ_{c}
2	1.304	1.409	1.411	$--$	0.79 ± 0.01
$\sqrt{3}$	1.222	1.344	1.367	1.369	0.83 ± 0.01
$\sqrt{2}$	1.084	1.207	1.241	1.253	0.88 ± 0.01
1	0.825	0.928	0.961	0.976	1.00 ± 0.01

Table 4: Maxima of $c_{\mathrm{eff}}(\lambda)$ in the limit $w, T \to \infty$ with fixed $\lambda = T^2/w$, as a function of system size L, for various values of n. We also show the estimates of the critical point λ_{c}, extrapolated to the $L \to \infty$ limit.

non-critical for any T. The interpretation in terms of RG flows is shown in Fig. 12. Note in particular that it is possible to flow directly from C to d, by perturbing C by a fine-tuned linear combination of the operators w and T^2, and that the dense-loop phase (i.e., the basin of attraction of D) only exists for $w > w_0$. For $n = \sqrt{2}$, we have determined $w_0 = 0.32 \pm 0.01$, corresponding to a temperature $T_0 = 0.92 \pm 0.01$.

Let us finally examine the properties of the point d'. As discussed above, we must take the limit $w, T \to \infty$ with $\lambda = T^2/w$ fixed in order to see competition between FPL configurations (with weight $\sim w^{N/2}$, where N is the number of vertices of the lattice) and empty space (with weight T^N). In this limit, the participating configurations consist of loops along which E_0 and non-E_0 edges alternate. An E_0-edge not covered by a loop carries a weight λ. This reformulation allowed us to write a transfer matrix for this limit, with parameters λ and n (the loop weight).

In Fig. 14 we display a plot of $c_{\mathrm{eff}}(\lambda)$ at $n = \sqrt{2}$. As $\lambda \to 0$ we recover the point P with $c = 1/2$, and in the large-λ limit non-critical behaviour is signaled by $c_{\mathrm{eff}} = 0$. A maximum at $\lambda = \lambda_{\mathrm{c}} \simeq 0.88$ corresponds to the critical behaviour of the point d'. The sharpening of the maximum with increasing L shows its repulsiveness in the variable $\lambda - \lambda_{\mathrm{c}}$.

In Table 4 we locate the point d' for several values of n and we give the corresponding values of the central charge. The latter prompt us to conjecture that the universality class of d' is that of a superposition of dilute loops and a critical Ising model, referred to
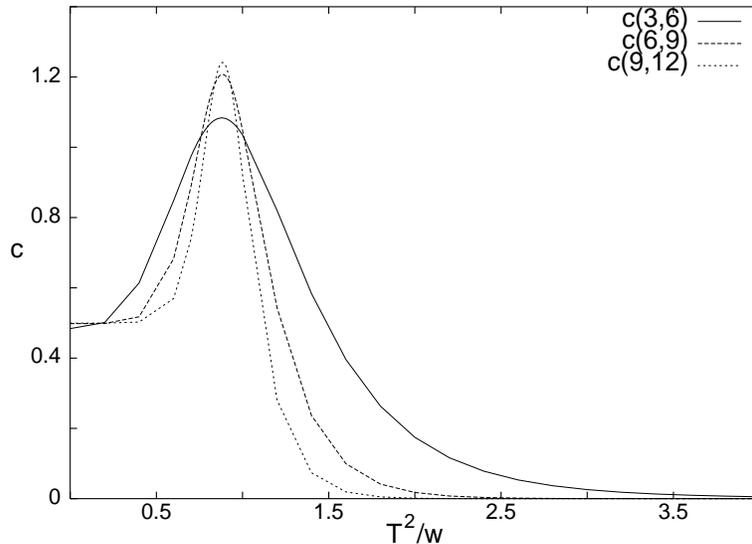
Figure 14: c_{eff} as a function of $\lambda = T^2/w$ with $T, w \to \infty$ and fixed $n = \sqrt{2}$.

n	$x_T(3)$	$x_T(6)$	$x_T(9)$	$x_T(12)$
2	0.7106	0.4975	0.4200	0.3685
$\sqrt{3}$	0.8509	0.6094	0.5411	0.4998
$\sqrt{2}$	1.1245	0.7805	0.7203	0.6886
1	$--$	1.1082	1.0435	1.0237

Table 5: Thermal exponent x_T at the point d', as a function of system size L, for various values of n.

as branch 4 in Ref. [23]. In other words,

$$c = \frac{3}{2} - \frac{6e_0^2}{1 + e_0}. \tag{6.9}$$

We have verified that the point d' can be detected as in Fig. 14 for $0 \leq n < 2$.

As to the thermal exponent, one would expect x_T to be the least of the values given by Eqs. (5.25) and (6.6). Curiously, this is not brought out by the data of Table 5. And the numerical data reported in Table 3 of Ref. [23] for branch 4 of the triangular-lattice $O(n)$ model agree neither with the theoretical expectation, nor with the data of Table 5.

6.3   Coulomb gas arguments for multicritical behaviour

Among the various critical branches identified for the $O(n)$ models on the square [24] and the triangular [23] lattices, and for the hexagonal-lattice $O(n)$ model in a staggered field [here], four appear to be generic. Those are dense (D) and dilute (d) loops, and their respective superpositions with a critical Ising model (D' resp. d').

In Ref. [39], it was explained how these four branches may be recovered in a more general setting from Coulomb gas arguments. The reasoning given in Ref. [39] applies to the square lattice, but can be readily adapted to the triangular-lattice O(n) model defined in Fig. 3.

Indeed, consider a generalisation of the triangular-lattice O(n) model in which loops can be either black or white, with respective weights n_b and n_w. Each edge is covered by either a black or a white loop. At a vertex, two loops can cross only if they have different colours. This can again be illustrated by Fig. 3, but the vertices marked ρ_2 and ρ_4 now each correspond to two distinct vertices depending on how the white loops are interconnected. Clearly, the original model is recovered by setting $n_\mathrm{w} = 1$ and renormalising the weights of the "doubled" vertices.

The Coulomb gas is once again based on an interface model on the dual lattice. After orienting each loop, two-dimensional microscopic heights are defined, depending on the orientation and colour of each edge. On the square lattice, this construction was based on an edge-colouring model [39] (like in section 5) which defined loops as alternating sequences of two colours. This is not possible on the triangular lattice, as the lattice is not bipartite and loop lengths are not necessarily even [20]. The resulting height model, however, still exists and has the crucial property that the two loop colours define independent directions in the height space[9] (this construction—as well as the detailed arguments—is exactly the same as in Ref. [39]).

The arguments given in Ref. [39] thus go through, and show that the two loop colours lead to two independent one-component Coulomb gases in the continuum limit. Therefore, four critical branches arise depending on whether each loop colour is in the dense or in the dilute phase. In particular, setting $n_\mathrm{w} = 1$, the white loops add either 0 or 1/2 to the central charge, depending on whether they are in the dense or the dilute phase. Indeed, the dilute O($n_\mathrm{w} = 1$) model is nothing but a critical Ising model.

6.4   The case of $n = 2$

The loop weight $n = 2$ is somewhat special. At $w = 1$, the critical points D and d become identical and describe the Kosterlitz-Thouless point of the XY model. In the usual O(2) model, this point is the critical end-point of a line of low-temperature fixed points along which the exponents vary continuously.

Interestingly, this feature is not present in the loop model [43]; we recall that the latter is defined by a truncation of the full O(n) model, which is not innocuous at low temperature. Thus, in the whole region $0 < T < T^\pm(w = 1)$, the critical exponents are constant and equal to their values at $T^\pm(w = 1)$.[10] In particular, the thermal exponent is marginally irrelevant (resp. marginally relevant) for temperatures slightly below (resp. above) $T^\pm(w = 1)$.

For $w > 1$, the lines $T^-(w)$ and $T^+(w)$ are present, just as for other $n < 2$. In particular we find the D' critical point at $w_\mathrm{c} = 2.9 \pm 0.1$ and $T^-(w_\mathrm{c}) = 0.91 \pm 0.04$. Its central charge agrees well with the prediction of Eq. (6.5), which reads $c = 3/2$.

---

[9]This is in contrast with the appearance of an "unexpected" extra height component in the FPL models on the hexagonal [16] and square [17] lattices, which are both linked to edge-colouring models.

[10]Notice that in this respect the phase diagram reproduced in Ref. [41] is slightly misleading.

w	$c(6,9)$	$c(9,12)$	$x_1(9)$	$x_1(12)$	$x_T(9)$	$x_T(12)$	$T^-(w)$
1.6	1.46271	1.48616	0.2277	0.2249	0.7151	0.7231	0.43 ± 0.01
2.0	1.47149	1.48938	0.2303	0.2282	0.7226	0.7283	0.60 ± 0.01
2.9	1.47670	1.49182	0.2401	0.2411	0.7136	0.7150	0.91 ± 0.01
4.0	1.47452	1.49078	0.2401	0.2407	0.7051	0.7067	1.23 ± 0.01
6.0	1.46613	1.48739	0.2434	0.2441	0.6782	0.6786	1.70 ± 0.01
10.0	1.45331	1.48173	0.2645	0.2703	0.6186	0.6107	2.40 ± 0.01
40.0	1.43237	1.46268	0.3106	0.3169	0.4967	0.4655	5.46 ± 0.01

Table 6: Estimates of c_{eff}, x_1 and x_T along the $T^-(w)$ curve at $n = 2$, for various system sizes.

Moreover, from Eq. (6.9) we also expect a value of $c = 3/2$ at the point d'; the numerical data in Table 4 are consistent with this expectation. This opens for the interesting possibility that the part of the curve $T^-(w)$ that connects D' and d' may be a *line of fixed points* with $c = 3/2$.

The numerical data for c, x_T and x_1 shown in Table 6 are not inconsistent with this possibility. While c and x_1 are fairly constant along the proposed line of fixed points, x_T steadily decreases beyond $w > w_c$ (also note that the $w \to \infty$ limit of Table 6 is consistent with the value of x_T given in Table 5). However, if this scenario were indeed true, one should be able to identify an exactly marginal operator at D'. We plan to investigate this issue further in the future.

6.5   Hard hexagons and hard triangles: $n > 2$

When $w = 1$, taking the limit $T, n \to \infty$ with fixed $z = n/T^6$ transforms the model (1.5) into Baxter's model of hard hexagons [40, 38]. The role of the hexagons is played by the loops of length six, which may surround any of the hexagonal-lattice faces. As a function of their fugacity z there is a solid-to-liquid transition at $z = z_c = (11 + 5\sqrt{5})/2$ at which the model is exactly solvable. For $z \to \infty$ there is a coexistence of three completely ordered phases, in which the loops are fully packed and all surround faces with the same label. This may lead one to expect some connection with a three-state Potts model, along the lines of section 4. And actually the exact solution at $z = z_c$ shows [40] that the critical exponents of the hard hexagon model coincide with those of the three-state Potts model.

More recently, it was shown numerically [41] that this critical behaviour extends to a critical curve $z_c(n)$ existing for any $n > 2$. In particular, as $n \to 2_+$ one has $z_c(n) \to \infty$ (or $T \to 0$). This remarkable finding means that the Z_3 symmetry is felt even by the "soft" particles (loops of length longer than six) at finite n. The results of Ref. [41] can be interpreted in RG terms by assuming that there is a curve of RG flows along the curve $z_c(n)$ directed towards the critical fixed point at $n = \infty$. Note that an RG flow changing the symmetry related parameter n is possible exactly because at $n > 2$ the loop weight operator is no longer marginal.

In section 4 we have discussed how taking $w > 1$ breaks three-phase coexistence down to two-phase coexistence. One is thus led to conjecture that for $n > 2$ there will exist a
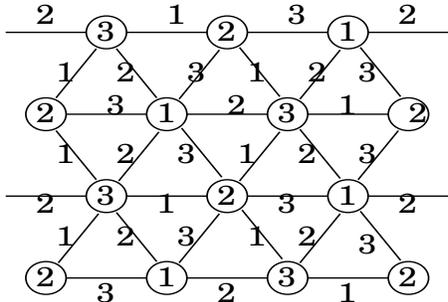
Figure 15: Triangular lattice obtained by superposing three shifted hexagonal lattices. The vertices (here surrounded by circles for clarity) and edges are labeled by integers $k = 1, 2, 3$ as shown.

critical manifold in the $w > 1$ half space that belongs to the Ising universality class (Z_2 type symmetry).

Let us consider more closely taking first $w \to \infty$, and then $T, n \to \infty$ with fixed $z = n/T^6$. Decimating the 2-faces as in section 2.2 we recover a model of *hard triangles*. These triangles are loops of length three that surround the faces of the triangular lattice; they may touch at the vertices, but not share an edge. The fugacity of a triangle is z. The two completely ordered states correspond to having all the triangles surround the faces labeled 1 or 3, respectively. It seems natural to conjecture that coexistence of these two states may lead to critical behaviour of the Ising type.[11]

We have checked these conjectures numerically. For any $n > 2$ we find that at $w = 1$ there exists a critical temperature $T_c(w = 1)$ with a $c = 4/5$ behaviour, consistent with the findings of Ref. [41]. For $w > 1$, this extends into a critical curve $T_c(w)$, with an RG flow directed towards larger w that eventually ends up in a $c = 1/2$ critical fixed point in the $w \to \infty$ limit. The location of this fixed point is such that $\lambda = T^2/w$ tends to a constant. This flow from $c = 4/5$ to $c = 1/2$ divides the phase diagram into a low-temperature ordered (solid) state and a high-temperature disordered (liquid) state; there appears to be no further critical points.

7 Loops on the triangular lattice

We finally consider several non-standard FPL models on the triangular lattice. These loop models exhibit different critical behaviour than the standard FPL model on the triangular lattice, which is in the universality class of dense loops [18, 20].

Consider constructing a triangular lattice by superposing three shifted hexagonal

---

[11]In order to compare with the conventional formulation of models of hard particles, it is useful to consider the dual lattice. The particles of fugacity z now occupy the vertices of the hexagonal lattice, and the hard-core constraint is that no two neighbouring vertices can be occupied. In this sense, the model is one of hard *squares* whose centres live on the hexagonal lattice. Note that this is different from the hard squares model where the particles live on the square lattice. Neither of these models appear to have been exactly solved.
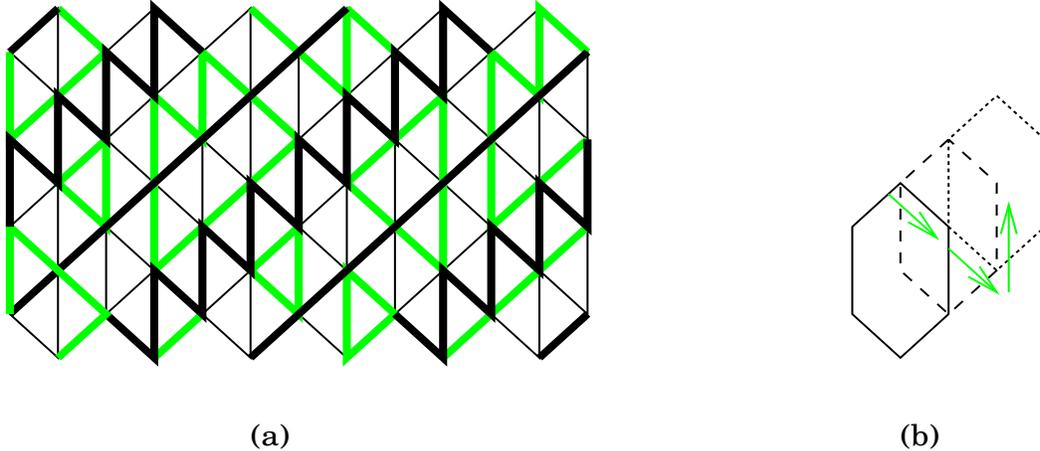
(a)   **(b)**

Figure 16: (*a*) The thick grey loops are the RGB loops. (*b*) The three hexagonal lattices are shown by the continuous, broken, and dotted lines respectively. Following successive dimers along edges on these three lattices, as shown by the arrows, one gets an RGB loop.

lattices, as shown in Fig. 15. The vertices of the triangular lattice are labeled $k = 1, 2, 3$ so that no two adjacent vertices have the same label. Let (k_1, k_2, k_3) be any permutation of $(1, 2, 3)$. Then the k_1'th hexagonal lattice consist of those edges of the triangular lattice that join vertices labeled k_2 and k_3. Conversely, at a triangular-lattice vertex labeled k_1, the hexagonal lattices labeled k_2 and k_3 share a common vertex. Each edge of the triangular lattice belongs to exactly one of the three hexagonal lattices.

7.1 The RGB model

The first model we consider is known as the red-green-blue (RGB) model, and was introduced and studied in Refs. [21, 22]. It is obtained by superposing independent dimer coverings of each of the three hexagonal lattices. We shall here study the more general case where the hexagonal lattices are endowed with three-colouring configurations, cf. section 2.1, each *BC*-type loop being weighted by n. Dimers correspond to colours A, and to weigh each dimer configuration equally we simply set $n = 1$. The dimers now form closed loops—the RGB loops—which are each weighted by unity. Apart from being fully packed, the RGB loops have the interesting properties that their length is always a multiple of three, and that they never make $\pi/3$ turns. An example is shown by the thick grey loops in Fig. 16(*a*) (disregard for the moment the other two kinds of loops shown).

In Ref. [22] a one-dimensional height model was associated with the RGB loops as follows. Imagine starting at a definite vertex of the triangular lattice, and traversing the RGB loop that goes through this vertex by moving in the clockwise direction. Each edge on the trajectory is a dimer on one of the three hexagonal lattices, and when tracing out the loop we note sequentially the labels of the hexagonal lattices to which each of these dimers belongs. If this sequence of labels is $123123\cdots$, or a cyclic permutation thereof, we shall call the RGB loop clockwise oriented; otherwise it is anticlockwise oriented. These

orientations can be used to define a one-dimensional height on the lattice faces, which we shall refer to as the *RGB height*. Properties of this height were studied in Ref. [22].

Note however that the orientation constructed above is not an *intrinsic* property of the RGB loops: unlike the orientation of BC-type loops defined in section 2.1, the RGB orientation is fixed once the trajectory of the corresponding loop has been fixed. For this reason we shall in the following rather focus on the orientations of the BC-type loops, and on the associated height mapping.

Since the three copies of the fully-packed hexagonal-lattice $O(n = 1)$ model do not interact, the critical properties of RGB loops are easily found. The free energies and the central charges of the three copies simply add up, and in particular one has

$$c = 3. \tag{7.1}$$

The same is true for critical exponents linked to vortex-type defects. Correlation functions in the RGB model are products of those in the individual hexagonal-lattice models. So once a given defect configuration on the triangular lattice has been decomposed into defects in the three hexagonal-lattice models, the corresponding critical exponents just need to be summed up.

In Fig. 17 we show a few examples. We first consider the thermal exponent on the triangular lattice, which is associated with an empty vertex. The corresponding vortex configuration, shown in Fig. 17(a), is equivalent to two one-string defects on the two hexagonal lattices which meet at the centre of the vortex. Thus, from Eq. (5.14),

$$x_T^{\mathrm{tri}} = x_1^{\mathrm{hex}} + x_1^{\mathrm{hex}} = \frac{1}{2}. \tag{7.2}$$

Note that this is different from x_T of the $n = 1$ FPL models on the hexagonal and the square lattices (which have $x_T = 1$ and $x_T = 2/3$ respectively). Also, in order for the energy-energy correlation function to have zero total magnetic charge on *each* hexagonal lattice, the two thermal defects have to placed on triangular-lattice vertices carrying the same label.

Next, consider the *bend defect* associated with a loop turning by an otherwise forbidden angle of $\pm\pi/3$. As all non-defect turns go through angles of $\pm 2\pi/3$, it is easy to show that a loop cannot close if there is only one $\pm\pi/3$ defect. We henceforth consider an RGB loop with two such defects, situated at distant points, and corresponding to angles $+\pi/3$ and $-\pi/3$ of opposite sign. The vortex due to one of these defects is shown in Fig. 17(b): it amounts to a one-string defect on either of two hexagonal lattices, just as in the case of the thermal defect. This leads to

$$x_{\pm\pi/3}^{\mathrm{tri}} = x_1^{\mathrm{hex}} + x_1^{hex} = \frac{1}{2}. \tag{7.3}$$

The one-string defect on the triangular lattice is shown in Fig. 17(c). It is seen to be equivalent to a one-string defect on one hexagonal lattice and no other defects on the other hexagonal lattices. The critical exponent is therefore

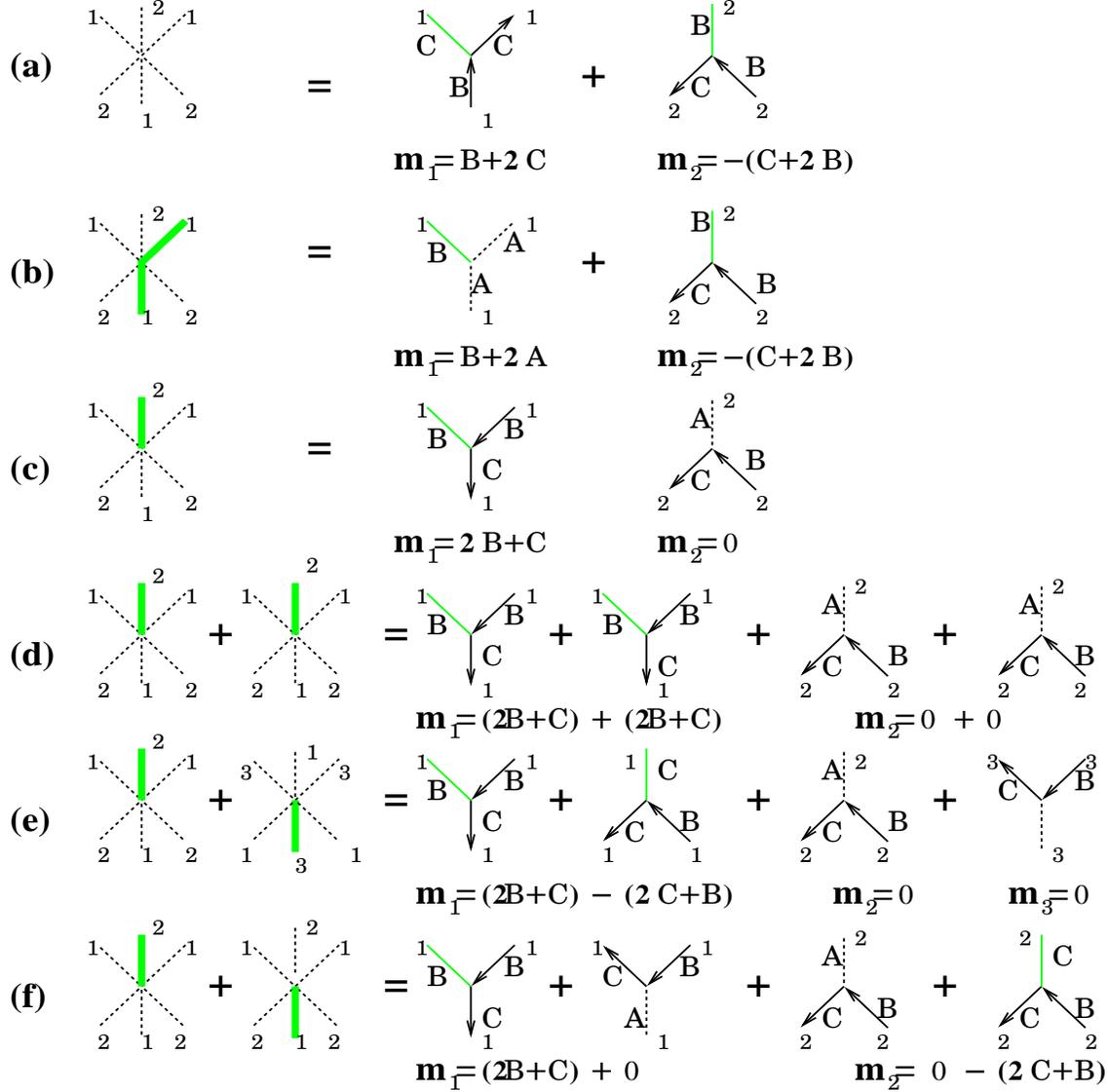$$x_1^{\mathrm{tri}} = x_1^{\mathrm{hex}} = \frac{1}{4}. \tag{7.4}$$

Figure 17: Defect vortices on the triangular lattice (left) and on the hexagonal lattice (right), with the corresponding magnetic charges. (a) Thermal defect, (b) the $\pm\pi/3$ bend defect, (c) one-string defect, (d)–(f) various examples of two-string defects (see text). On the left, the RGB loops on the triangular lattice are shown in thick grey linestyle, and the empty bonds by dotted lines. On the right, the string defects on the hexagonal lattices (with labels as shown) are given in thin grey linestyle; non-defect directed loops are black. The magnetic charges on the two sublattices are denoted by $\mathbf{m}_1$ and $\mathbf{m}_2$.

As discussed earlier, the fractal dimension D_{f} of a loop is such that $2 - D_{\mathrm{f}}$ (the codimension) is the critical exponent describing the decay of the probability that two distant points belong to the same loop [32, 33]. In a model of oriented loops, this critical exponent can be computed by reversing the direction along one half of the loop, whence it becomes identified with x_2 as in Eq. (5.15). In the present case, the RGB loops do not possess an intrinsic orientation, as discussed above, and the two points must be marked in another way. A convenient way is by inserting the bend defect of Fig. 17(b). We therefore arrive at

$$D_{\mathrm{f}} = 2 - x^{\mathrm{tri}}_{\pm\pi/3} = \frac{3}{2}. \tag{7.5}$$

This agrees with earlier numerical work [42]. Note that this is different from D_{f} of the $n = 1$ FPL models on the hexagonal and the square lattices (which both have $D_{\mathrm{f}} = 7/4$).

There are several different ways of making two strings emanate from nearby, but distinct points. The corresponding critical exponents are thus *not* linked to D_{f}, and moreover depend on the exact geometry of the string insertions, even though macroscopically the two strings appear to have common end-points. We illustrate this comment by a few examples.

Consider first the geometry of Fig. 17(d) in which the two nearby defects reside on the same sublattice and have the same alignment. The defect charge is equivalent to that of two nearby one-string defects on one hexagonal lattice, and leads to $x^{\mathrm{tri}}_{(d)} = x^{\mathrm{hex}}(\mathbf{e}_0, 2(2\mathbf{B} + \mathbf{C})) = 5/4$, by Eq. (5.8).

A different alignment of the strings is shown in Fig. 17(e)–(f). If the two defects reside on different sublattices, as in Fig. 17(e), one obtains $x^{\mathrm{tri}}_{(e)} = x^{\mathrm{hex}}(\mathbf{e}_0, (\mathbf{B} - \mathbf{C})) = 1/4$. If they are on the same sublattice, as in Fig. 17(f), one has $x^{\mathrm{tri}}_{(f)} = 1/2$.

7.2 The triple RGB model

A more exotic model can be obtained if we set $n = 2$, so as to weigh equally the three-colouring configurations (rather than the dimer coverings) on each of the three hexagonal lattices. Each vertex on the triangular lattice is now visited by three distinct RGB-type loops, having respective colours A, B and C.

A sample configuration is shown in Fig. 16(a), where the A-loops appear as thick grey lines, the B-loops as thick black lines, and the C-loops as thin black lines. The central charge of this model is now $c = 3 \times 2 = 6$.

Again, we emphasise that the three copies of the $n = 2$ hexagonal-lattice FPL model are completely decoupled, and critical exponents can be obtained along the lines laid out above.

7.3 Staggered models

Yet other models can be obtained by taking the $w \to \infty$ limit in one or several of the superposed hexagonal-lattice FPL models. As we have seen in section 3.5 this will eliminate one unit of central charge from each of the concerned models.

We recall that infinite w means that the E_0-type edges cannot have the colour A. Thus, within the RGB model one obtains critical theories with $c = 2$, 1 or 0, depending on whether the loops are excluded from the E_0 edges on one, two or three hexagonal lattices. Similarly, within the triple RGB model one gets $c = 5$, 4 or 3, depending on whether the A-coloured RGB loops are excluded from the E_0 edges on one, two or three hexagonal lattices. In all cases, critical exponents can be worked out as usual.

8 Conclusion

In this paper, we have studied the loop model (1.5) on the hexagonal lattice subjected to a staggered field w. The parameter w breaks down the three-phase coexistence present at $w = 1$ and has an interesting competition with the temperature T.

We have found that the model has four new critical branches for $w \neq 1$, as seen in Fig. 12. Three of these exist for $0 \leq n \leq 2$ and are denoted by P (Potts model), D' (tricritical dense loops) and d' (tricritical dilute loops). Furthermore, there is a fourth critical point for $n > 2$ belonging to the Ising universality class. These are in addition to the four old branches known to exist at $w = 1$: C (compact loops), D (dense loops) and d (dilute loops) for $|n| \leq 2$; and the critical three-state Potts model for $n > 2$.

It seems that the multicritical branches D' and d' are as generic as the D and d branches, since all of these have previously been found on the square and triangular lattice $O(n)$ models. An explanation of this universality is given within the Coulomb gas formalism in section 6.3. On the other hand, the point C (compact loops, $T = 0$ and $w = 1$) is specific to the hexagonal lattice. Due to the enhanced symmetry, its Coulomb gas is based on a two-component height field, and this is unstable towards both the perturbations in T and in w.

A part of our results can be explained via the embedding of the model (1.5) into the more general triangular-lattice $O(n)$ model. However, the classification of possible types of critical behaviour in this latter model [23] does not appear to be complete. In particular, compact loops and the RGB model are interesting special cases of the triangular-lattice $O(n)$ model which are not accounted for in Ref. [23].

It should be emphasised that even though the $O(n)$-type loop models on various lattices (hexagonal, square and triangular) share many universal features, they also fail to account for some aspects of the low-temperature physics of the original $O(n)$ spin model. For example, the generic symmetry-broken low-temperature Goldstone phase is absent [9, 10], and for $n = 2$ there is no line of critical points below the Kosterlitz-Thouless temperature [43].

Finally, we have also studied constrained compact RGB-type loops on the triangular lattice. In particular, we have proved that RGB loops have the fractal dimension $D_{\mathrm{f}} = 3/2$. This finding would seem to indicate that these loops are level lines of a Gaussian surface. More precisely, we conjecture that the RGB height (defined in section 7.1) defines a Gaussian surface.

Interestingly, our derivation of the value of D_{f} is based on level lines of three different four-dimensional surfaces which are manifestly non-Gaussian. It would be interesting if one could find a more direct derivation, in terms of the RGB height.

Acknowledgments

References

[1] P. G. de Gennes, Phys. Lett. A **38**, 339 (1972).

[2] J. Zinn-Justin, *Quantum field theory and critical phenomena* (Clarendon Press, Oxford, 1989).

[3] E. Domany, D. Mukamel, B. Nienhuis, and A. Schwimmer, Nucl. Phys. B **190**, 279 (1981).

[4] B. Nienhuis, Phys. Rev. Lett. **49**, 1062 (1982).

[5] R. J. Baxter, J. Phys. A **19**, 2821 (1986).

[6] H. Saleur, J. Phys. A **19**, L807 (1986).

[7] M. T. Batchelor and H. W. J. Blöte, Phys. Rev. Lett. **61**, 138 (1988); Phys. Rev. B **39**, 2391 (1989).

[8] B. Duplantier and H. Saleur, Nucl. Phys. B **290**, 291 (1987).

[9] N. Read and H. Saleur, Nucl. Phys. B **613**, 409 (2001).

[10] J. L. Jacobsen, N. Read and H. Saleur, Phys. Rev. Lett. **90**, 090601 (2003).

[11] G. Parisi and N. Sourlas, J. de Physique Lettres **41**, L403 (1980).

[12] N. Yu. Reshetikhin, J. Phys. A **24**, 2387 (1991).

[13] H. W. J. Blöte and B. Nienhuis, Phys. Rev. Lett. **72**, 1372 (1994).

[14] R. J. Baxter, J. Math. Phys. **11**, 784 (1970).

[15] M. T. Batchelor, J. Suzuki and C. M. Yung, Phys. Rev. Lett. **73**, 2646 (1994).

[16] J. Kondev, J. de Gier and B. Nienhuis, J. Phys. A **29**, 6489 (1996).

[17] J. L. Jacobsen and J. Kondev, Nucl. Phys. B **515**, 701 (1998).

[18] M. T. Batchelor, H. W. J. Blöte, B. Nienhuis and C. M. Yung, J. Phys. A **29**, L399 (1996).

[19] S. Higuchi, J. Phys. A **32**, 3697 (1999).

[20] J. L. Jacobsen, J. Phys. A **32**, 5445 (1999).

[21] I. Benjamini and O. Schramm, unpublished, cited in Ref. [22].

[22] D. B. Wilson, *On the Red-Green-Blue model*, cond-mat/0212042.

[23] Y. M. M. Knops, B. Nienhuis and H. W. J. Blöte, J. Phys. A **31**, 2941 (1998).

[24] S. O. Warnaar, M. T. Batchelor and B. Nienhuis, J. Phys. A **25**, 3077 (1992).

[25] P. W. Kasteleyn and C. M. Furtuin, J. Phys. Soc. Japan **26** (Suppl.), 11 (1969); C. M. Fortuin and P. W. Kasteleyn, Physica **57**, 536 (1972).

[26] R. J. Baxter, J. Phys. C **6**, L445 (1973).

[27] J. L. Cardy and J. L. Jacobsen, Phys. Rev. Lett. **79**, 4063 (1997).

[28] A. B. Zamolodchikov, Pis'ma Zh. Eksp. Teor. Fiz. **43**, 565 (1986). [JETP Lett. **43**, 730 (1986).]

[29] B. Nienhuis, in *Phase transitions and critical phenomena*, edited by C. Domb and J. L. Lebowitz (Academic Press, London, 1987), Vol. 11.

[30] P. D. Francesco, P. Mattieu and D. Sénéchal, *Conformal field theory* (Springer Verlag, New York, 1997).

[31] Vl. S. Dotsenko and V. A. Fateev, Nucl. Phys. B **240**, 312 (1984); *ibid.* **251**, 691 (1985).

[32] H. Saleur and B. Duplantier, Phys. Rev. Lett. **58**, 2325 (1987).

[33] J. Kondev, C. L. Henley and D. G. Salinas, Phys. Rev. E **61**, 104 (2000).

[34] H. W. J. Blöte and B. Nienhuis, J. Phys. A **22**, 1415 (1989).

[35] H. W. J. Blöte, J. L. Cardy and M. P. Nightingale, Phys. Rev. Lett. **56**, 742 (1986).

[36] I. Affleck, Phys. Rev. Lett. **56**, 746 (1986).

[37] J. L. Cardy, J. Phys. A **17**, L385 (1984).

[38] R. J. Baxter, *Exactly solved models in statistical mechanics* (Academic Press, New York, 1982).

[39] J. L. Jacobsen and J. Kondev, J. Stat. Phys. **96**, 21 (1999).

[40] R. J. Baxter, J. Phys. A **13**, L61; *ibid.* **19**, 2821 (1986); *ibid.* **20**, 5241 (1987).

[41] W. Guo, H. W. J. Blöte and F. Y. Wu, Phys. Rev. Lett. **85**, 3874 (2000).

[42] R. W. Kenyon and D. B. Wilson, unpublished (1999), cited in Ref. [22].

[43] H. W. J. Blöte and B. Nienhuis, Physica A **160**, 121 (1989).